Earthq Eng & Eng Vib (2021) 20: 747-770 **DOI**: https://doi.org/10.1007/s11803-021-2050-7

Seismic performance of precast bridge columns connected with grouted corrugated-metal duct through biaxial quasi-static experiment and modeling

Xia Zhanghua[1†], Lin Shangshun[2‡], He Yongbo[1†], Ge Jiping[3†] and Sun Jinlei[1†]

1. *Department of Civil Engineering, Fuzhou University, Fuzhou 350116, China*
2. *Department of Civil Engineering, Fujian University of Technology, Fuzhou 350116, China*
3. *Department of Civil Engineering, Shanghai Institute of Technology, Shanghai 201418, China*

Abstract: In this paper, the seismic behaviors of precast bridge columns connected with grouted corrugated-metal duct (GCMD) were investigated through the biaxial quasi-static experiment and numerical simulation. With a geometric scale ratio of 1:5, five specimens were fabricated, including four precast bridge columns connected with GCMD and one cast-in-place (CIP) bridge column. A finite element analysis model was also established by using OpenSees and was then calibrated by using the experimental results for parameter analysis. The results show the biaxial seismic performance of the precast bridge columns connected with GCMD was similar to the CIP bridge columns regarding ultimate bearing capacity and hysteresis energy, and further, that it could meet the design goal of equivalent performance. The seismic performance of the precast bridge columns connected with GCMD deteriorated more significantly under bi-directional load than under uni-directional load. A proper slenderness ratio (e.g., 7.0–10.0) and longitudinal reinforcement ratio could significantly improve the energy dissipation capacity and deformation capacity of the precast bridge columns, while the axial load ratio and concrete strength had little influence on the above properties. The research results could bring insights to the development of the seismic design of precast bridge columns connected with GCMD.

Keywords: precast bridge column; cast-in-place column; grouted corrugated-metal duct connection; biaxial quasi-static test; seismic performance; hysteresis energy

1 Introduction

Precast bridge columns have been widely used to achieve rapid construction without affecting traffic flow (Wacker *et al.*, 2005). Mainly, they have been studied and practiced in the United States, New Zealand, and China (Wang *et al.*, 2010; Motaref *et al.*, 2011; Palermo and Mashal, 2012; Chan *et al.*, 2016; Qu *et al.*, 2018). Due to the advantages of rapid construction, reliable performance and larger construction tolerances (Pang *et al*., 2009; Steuck *et al*., 2009), the grouted reinforcing bar connections, commonly known as grouted bar-in-conduit or corrugated duct connections, are widely used to connect precast bridge columns (Elsayed *et al*., 2018). In recent years, with the advantages of convenient construction, low risk of slurry leakage and low costs, grouted corrugated-metal duct (GCMD) is commonly used.

The method employed to connect precast bridge columns with GCMD is to embed the metal ducts in a pile cap or a bent cap, reserve some space for exposed longitudinal reinforcement in the bridge column, and grout high-strength mortar into the metal ducts when assembling the bridge columns on site. This connection is mainly used when the column is connected to the pile cap or the bent cap. In the United States, it is mainly used between the column and the bent cap area in bridges such as the Belton Lake Bridge and the Rehab Lake Bridge (Restrepo *et al.*, 2011).

To prevent the main rebar from being pulled out of the duct, it is critical to ensure a proper bond between GCMD and steel bars. Darwin and Zavaregh (1996) studied the bond-anchorage mechanism of GCMD and analyzed the factors affecting its bond-anchorage performance, including the anchor length of the steel bars, the grout performance, and the diameter and thickness of the duct. The results showed that the bond strength provided by grouts was insensitive to hole

Correspondence to: Lin Shangshun, Department of Civil Engineering, Fujian University of Technology, Fuzhou 350116, China
Tel: +86-13665055108
E-mail: linshangshun@fjut.edu.cn
†Associate Professor; ‡Professor

Supported by: National Natural Science Foundation of China under Grant No. 51408360, the Natural Science Foundation of Fujian (NSFF) under Grant No. 2020J01477 and the Technology Project of Fuzhou Science and Technology Bureau (TPFB) under Grant No. 2020-GX-18
Received November 13, 2019; **Accepted** July 29, 2020

diameter, while it rose with increasing embedment length, cover, and steel bar size. Brenes *et al.* (2006) performed pullout tests on thirty-two samples of precast bridge columns connected with GCMD. They found that the tensile capacity of the connector was insensitive to the epoxy coating on the connector or the presence of transverse spiral bars around a group of connectors. It was sensitive to several factors, including the type of duct, the embedded length of the connector, the number of connectors tested simultaneously in tension, and the placement of the connector within the duct. By contrast, Raynor *et al.* (2002) found that GCMD provided a higher bond strength than conventional concrete. Steuck *et al*. (2007) systematically studied the effects of steel bar diameter, anchor length and steel fiber on the connection between GCMD and steel bars. In their study, the diameter was proved to play a minor role and the addition of fibers to the grout reduced the bond strength of the GCMD. Raynor *et al.* (2002) studied the relationship between bond stress and slip through the use of a quasi-static test. Next, they proposed and verified the displacement equation of the loading end, thereby confirming the bond reliability of the GCMD. Currently, the Shanghai government has specified the design calculation of the metal ducts in connection and has issued a technical regulation (DG/TJ 08-2160-2015) for precast bridge columns in medium and low-intensity seismic zones.

In order to analyze the seismic performance of precast bridge columns connected with GCMD, Pang *et al.* (2010) conducted a quasi-static test of segmental columns with GCMD. The results showed that the load-displacement response and damage evolution of the GCMD-connected precast bridge column were close to those of the cast-in-place (CIP) bridge column. Khaleghi *et al.* (2012) introduced the successful application of a double-column pier top and a bent cap with GCMD in the precast bridge column in Washington State, in addition to providing corresponding quasi-static experiment results. Tazarv and Saiidi (2015, 2016, 2017) conducted a quasi-static test on two precast bridge column models. The results showed that the connection performance of GCMD with ultra-high-performance concrete (UHPC) was better than that of a traditional CIP connection. Wang *et al.* (2018) studied the seismic performance of the precast bridge columns connected to GCMD with prestressed tendons by using a quasi-static test that considered the effects of bonding, prestressed tendons, and prestressed rods. For the component with bonding prestress, its strength was increased while its energy dissipation capacity was reduced. For the component without bonding prestress, its energy dissipation capacity was not compromised, but its ductility was reduced. The present uniaxial quasi-static study found that the precast bridge column connected with GCMD demonstrated a good seismic performance, and the ultimate load and deformation capacity were close to those of the corresponding CIP bridge column.

The above studies mainly focus on the understanding of seismic performance through the bond-anchorage test and the uniaxial quasi-static test, while the bridge columns were often subjected to compression and biaxial bending action due to earthquakes. It has been shown that the reinforced concrete bridge columns have bi-directional coupling effects under biaxial bending (Park, 1989; Qiu *et al.*, 2002). Damage to the bridge column in one direction could result in a decrease in strength and stiffness in the other direction, thereby compromising its seismic performance. Thus, it is necessary to investigate the seismic performance of the precast bridge columns under the action of biaxial bending. Nevertheless, only a few studies have conducted biaxial quasi-static tests for precast bridge columns, and the seismic performance of the precast bridge columns connected with GCMD under bi-directional load remains unclear. Due to the connection joints, the seismic performance of precast bridge columns could be different when compared to the CIP bridge columns, especially under bi-directional load, which indicates a need for additional research.

This study initially conducted a biaxial quasi-static experiment to investigate the seismic performance of precast bridge columns connected with GCMD under bi-directional load. The failure modes and hysteresis characteristics of the bridge columns were analyzed and compared to those of the CIP bridge columns. The testing results were used to verify the accuracy of the finite element model (FEM), which was then used to perform a parameter analysis for greater understanding of the GCMD connected precast bridge columns with regard to the influence of axial load ratio, longitudinal reinforcement ratio and concrete strength on seismic performance. The comprehensive research results aimed to provide guidance for optimizing the seismic design of the precast bridge columns connected with GCMD while considering bi-directional load.

2 Experiment

2.1 Specimen design

The prototype in this paper had a section size of 2.5 m × 1.7 m, 84 longitudinal reinforcements with a diameter of 28 mm, a reinforcement ratio of 1.23%, a cover concrete thickness of 35 mm, a concrete strength grade of C40 (with the cubic compressive strength of 42.4 MPa, and an elastic modulus of 30,700 MPa). The design axial force was $\eta f_{cd} A = 0.1 \times 26{,}800 \times 4.21 = 11{,}283$ kN, where η is the axial compression ratio, A is the cross-sectional area, and f_{cd} is the design concrete compressive strength.

Five bridge column models, including one conventional cast-in-place (CIP) concrete bridge column (RC0) and four precast bridge columns connected with GCMD (BBPC-1, BBPC-2, BBPC-3, and BBPC-4), were designed with a scale ratio of 1:5. BBPC-1 and

BBPC-2 specimens had the same dimensions. Except for the height of the columns, the other dimensions of BBPC-3 and BBPC-4 were the same as those of BBPC-1 and BBPC-2 (Table 1). Figures 1(a)–1(c) show the dimensions of the test specimens. In Fig. 1, ① represents the longitudinal reinforcement and ②–④ are stirrups and ties.

Table 1 shows the main design parameters of the test specimens. BBPC-2 was chosen as the control specimen, and its seismic performance was designed to be identical to that of the CIP specimen. The effects of loading pattern and slenderness ratio on the seismic performance of the GCMD-connected precast bridge columns were investigated. The axial load ratios of all the specimens were the same as 0.1. The loading patterns of BBPC-1 and BBPC-2 were different (uni-directional load and rectangular load, respectively), while BBPC-2 and RC0 were both under the rectangular load. Except for the slenderness ratio, the other design parameters of BBPC-3 and BBPC-4 were the same as BBPC-2. The slenderness ratio λ is the ratio of the effective column height to the short side length of the section; the volume-stirrup ratio P_s refers to the ratio of the stirrup volume to the volume of the bridge column.

According to China′s current standard specifications (Code for Seismic Design of Urban Bridges, 2011), the metal duct consisted of circular stainless-steel and its length should not be less than $24d_s$ (d_s is the diameter of the connected longitudinal reinforcement). Note that the length here refers to the reinforcement anchorage length, not the bond length. The metal duct used to connect the precast bridge column specimens for testing was thus designed with a length of 540 mm, an inner diameter of 45 mm, an outer diameter of 47 mm, and a wall thickness of 0.6 mm. The depth of the longitudinal reinforcement embedded in the metal ducts was 540 mm, which was consistent with the length of the metal ducts.

Meanwhile, to meet the size of MTS anchor plate on the loading end, a loading head on the top of the specimens was designed as 530 mm × 700 mm × 700 mm. The footing was designed as 1,300 mm × 800 mm × 740 mm by considering the duct length, the position of the anchorage hole of the reaction wall and the effective height of the bridge column. The center of loading was 250 mm from the top of the bridge column.

By considering the test loading device, the effective height of the column was designed as the distance from the bottom of the column to the center of the loading head. Concrete with a strength grade of C40 was used for the loading head, column body and footing. HRB400 was used for longitudinal reinforcement. The longitudinal reinforcement of all specimens was

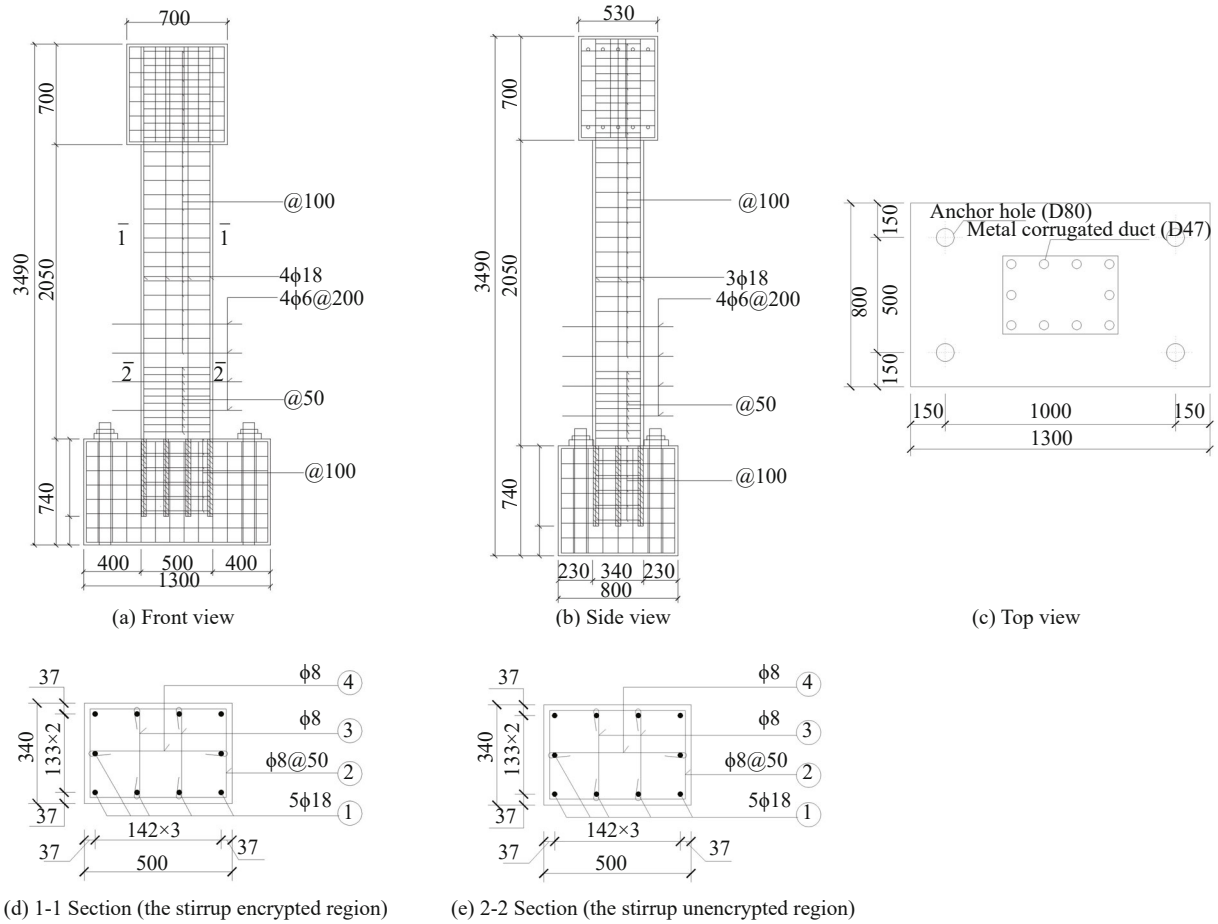

Fig. 1 Structural graph of the specimens (the unit of all dimensions is cm, except that the unit of the steel bar size is mm)

composed of 10Φ18 mm in the section, The transverse steel bar was applied with a rectangular stirrup Φ8 mm@100 mm in the unencrypted region, while the spacing between the stirrups was intensified to 50 mm in the bottom region within 500 mm from the surface of the footing (the encrypted stirrup region) of the precast bridge specimens. The thickness of the cover concrete was 20 mm.

The US AASHTO (2017) limitation requirements and China′s current standard specifications (Code for Seismic Design of Urban Bridges, 2011) indicate that the stirrup reinforcement ratio in the potential plastic hinge region of the columns can be respectively expressed by Eqs. (1) and (2). All five of the specimens in this study met these requirements. The stirrups of the bridge columns were designed according to the current requirements for restraint and shear resistance. The stirrups were made of HPB235 reinforcement bars with a diameter of 8 mm. The stirrup spacing of all specimens was less than six times the diameter of the longitudinal reinforcement.

$$P_s \geq 0.3\frac{f_c'}{f_{yh}}\left[\frac{A_g}{A_c}-1\right] \text{ and } P_s \geq 0.12\frac{f_c'}{f_{yh}} \tag{1}$$

$$P_s \geq \left[0.1\eta_k + 4.17(\eta_k - 0.1)(P_l - 0.01) + 0.02\right]\frac{f_c'}{f_{yh}} \tag{2}$$

where P_s is the stirrup reinforcement ratio, η_k is the axial load ratio, f_{yh} is the yield strength of the stirrup, A_c is the core concrete section area, P_l is the longitudinal reinforcement ratio, and P is the additional axial load.

The length of the potential plastic hinge region L_p recommended by the US AASHTO (2017) and China′s current standard specifications (Code for Seismic Design of Urban Bridges, 2011) was calculated according to Eqs. (3) and (4). The spacing of the encrypted stirrup region at the bottom of the column was set to 50 mm, and the spacing of the unencrypted region was set to 100 mm.

$$L_p \geq \max(b_{max}, 1/6h_0, 467 \text{ mm}) \tag{3}$$

$$L_p \geq \max(b_{max}, 1/6h_0, 500 \text{ mm}) \tag{4}$$

where b_{max} is the largest cross-sectional dimension and h_0 is the effective height of the bridge column.

2.2 Properties of concrete, reinforcement and UHPC materials

The specimens were made of commercial concrete with a strength grade of C40. The longitudinal reinforcement bar of the bridge column was made of HRB400 hot rolled steel with a diameter of 18 mm. The stirrups of the bridge column consisted of a HPB235 plain reinforcement bar with a diameter of 8 mm. The mechanical properties of the reinforcement steel bars were measured according to GB/T 228.1-2010 (2010). The results are shown in Table 2.

Ultra-high-performance concrete (UHPC) was used for filling the GCMD, which connects the precast bridge columns. Its mix proportion is presented in Table 3, where the volume ratio was assigned to steel fiber, and the mass ratio was set to other materials in which the cement mass was defined as 1. The fine sand had a maximum particle size of less than 0.63 mm. The superplasticizer was composed of CX-8 polycarboxylate, supplied by Fuzhou Chuangxian Engineering Materials Co., Ltd., and its water reducing rate was 25%. The 28-day compressive strength was 117 MPa, which meets the

Table 1 Main design parameters of the specimens

Group	Specimen No.	Effective height h_0 (m)	Height to width ratio R_b	Axial load ratio η_k	Slenderness ratio λ	Volumetric ratio of stirrup P_s (%)	Loading pattern
CIP bridge column	RC0	2.4	1.47	0.10	7.06	1.80	rectangular
Precast bridge columns connected with GCMD	BBPC-1	2.4	1.47	0.10	7.06	1.80	uni-directional
	BBPC-2	2.4	1.47	0.10	7.06	1.80	rectangular
	BBPC-3	1.4	1.47	0.10	4.12	1.80	rectangular
	BBPC-4	3.4	1.47	0.10	10	1.80	rectangular

Table 2 Measured properties of reinforcement

Reinforcement	Diameter (mm)	Yield strength (MPa)	Ultimate strength (MPa)	Elastic modulus (MPa)	Elongation (%)
Stirrup (HPB235)	8	241	330	212,000	26
Longitudinal reinforcement (HRB400)	18	412	567	213,000	31

technical specification for prefabricated bridge columns (DG/TJ 08-2160-2015).

2.3 Pullout test of the metal duct-steel bar connection

The good bond performance of UHPC grouting connection for reinforcement bars and ducts has been verified by Tazarv (Tazarv and Saiidi, 2016). This test mainly focused on the bond performance of the connection between the metal duct and concrete. Four metal duct-steel bar connection specimens were designed and tested according to the standard test method for concrete structures (GB/T 50152-2012) and the standard test method for splitting the tensile strength of cylindrical concrete specimens (ASTM, 2011). The bottom of the specimens consisted of a concrete cube with a side length of 180 mm and a strength grade of C40. The reinforcement bar was 500 mm long and was made of HRB400 with a diameter of 18 mm. The ducts were filled with UHPC to connect the longitudinal reinforcement bars. The unbonded section was 90 mm long and separated from the normal concrete (C40) by plastic foam. The detailed design of the component is shown in Fig. 2. The universal testing machine used for loading had a loading speed of 9.72 kN/min. The materials used in the metal duct-steel bar connection specimens were the same as those used in all test specimens. Thus, the material mechanical properties of the specimens were the same, as shown in Tables 2 and 3.

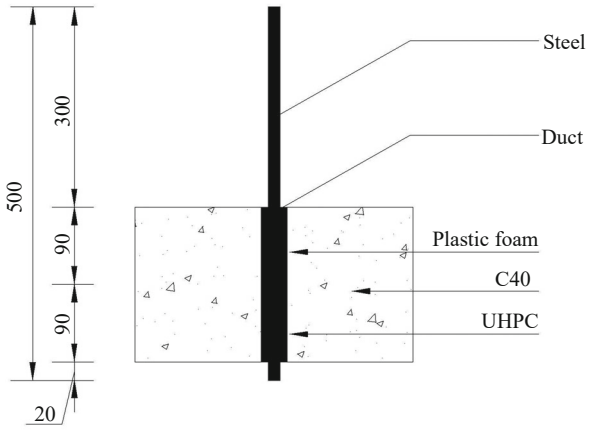

Fig. 2 Illustration of metal duct-steel bar connection specimens (unit: mm)

During the test, the splitting failure of the specimens was observed and a slip between the steel bars and the ducts was not found, indicating a good bond performance among the specimens. The average maximum splitting failure load of the other four specimens was 79.77 kN (see Table 4), which could be regarded as the limit value for the splitting failure of the specimens. The results show that the metal duct-steel bar connection specimens were not pulled out from concrete, indicating that the UHPC grouting duct would provide a good connection between the column and the footing for the bridge column specimens. This result was also verified in the quasi-static test.

2.4 Experiment scheme

2.4.1 Loading devices and loading scheme

The quasi-static test of all five specimens was performed in Experimental Hall 2 of the Civil Engineering College at Fuzhou University. An MTS244.31 250 kN actuator and an MTS244.41 500 kN actuator made by MTS (Mechanical Testing & Simulation) were used as loading devices. A high-precision hydraulic jack with a range of 1,000 kN was used to provide a constant axial load for the specimens. The lower part of the jack device was supported on a spherical hinge to ensure that the load applied by the jack was always vertically downward. The on-site layout of the loading devices is shown in Fig. 3, where the west and south sides of the specimen are presented.

The displacement loading protocols in this experiment were based on the seismic test guideline JGJ/T 101-2015 (2015). The uni-directional load was applied to the RC0 specimen along the strong axis (X direction). Figure 4 shows the uni-directional load protocol. In the elastic stage, the displacement was loaded with 1 mm at the first level, and the loading displacement was increased by an interval of 2 mm in the following level before the steel bar yielded, and each cycle was repeated once in this stage. After the steel bar yielded, the loading displacement was incremented by 10 mm. The loading cycle was performed three times and was terminated until the transverse strength of the specimen was reduced to 85% of its maximum strength.

Table 3 UHPC mix proportion

Steel fiber (V%)	Water binder ratio	Cement (V%)	Silica fume (V%)	Fine sand (V%)	Superplasticizer (V%)
3	0.18	1	0.3	1.20	0.025

Table 4 Pullout test results

Specimen No.	1	2	3	4	5	6
Maximum force (kN)	77.8	115	82.4	84.6	59.2	74.3

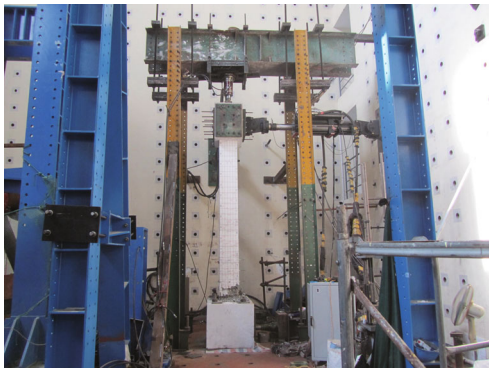

(a) Loading device and sample

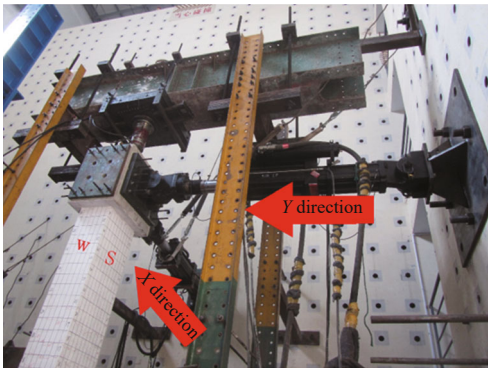

(b) West and south sides and loading at *X*/*Y* direction

Fig. 3 Photos of on-site layout and sample details with loading directions

Rectangular displacement loading was performed on the four precast segmental specimens, and the ratio of displacement in *X* direction to that in *Y* direction was 1:1, as shown in Fig. 5. During the test, the displacement and load on the top of the bridge column were recorded by an MTS actuator. The loading process included two stages. In the elastic stage, the displacement was first simultaneously loaded to 1 mm in *X* and *Y* directions, and the displacement was increased by an amplitude of 2 mm with one cycle. When the steel bar yielded, the displacement was increased by 10 mm, and the loading cycle repeated three times. The loading was terminated when the load capacity of the specimen dropped to 85% of its maximum load.

2.4.2 Measuring points layout of displacement

The displacement at the top of the bridge column, the sliding displacement of the pile cap and the opening-closing extent at joints were measured in this study. The displacement at the top of the bridge column was measured by the sensors of an MTS electro-hydraulic servo loading system, while the others were measured by strain-type displacement sensors. The displacement measuring points of the five specimens can be seen in Table 5, while Fig. 6 shows the measurement points in the plastic hinge region, the sliding displacement of cap and the opening-closing extent of joints. The displacement drift ratio at the top of the bridge column was used to indicate the horizontal relative deformation of a bridge column. The displacement drift ratio of the column in this study is defined as the ratio of the displacement at the top of the column to the effective height. The residual deformation is determined as the plastic deformation when the loading is unloaded as zero.

The load-displacement data were then used to produce the hysteresis loop. The enclosed area of the load-displacement (*P*-*Δ*) curve in the hysteresis loop represents the amount of energy absorbed by the structure under external loads such as that resulting from an earthquake. The higher the energy dissipation index is, the stronger the energy dissipation capacity

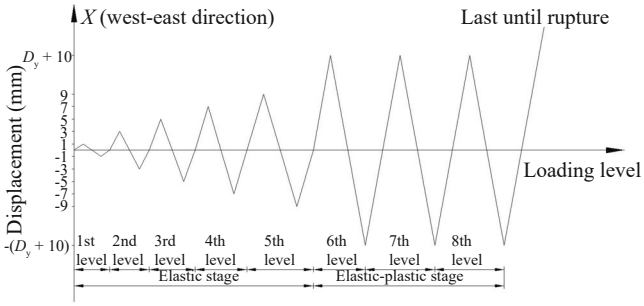

Fig. 4 Uni-directional load system

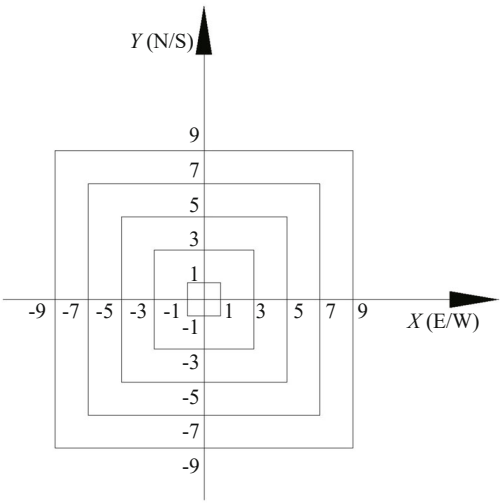

Fig. 5 Bi-directional rectangular load system

of the specimen will be, and the better the seismic performance. Hysteresis energy dissipation capacity E_x and E_y in *X* and *Y* directions can be calculated by Eqs. (5) and (6), respectively.

$$E_x = \int P_x d_x \tag{5}$$

$$E_y = \int P_y d_y \tag{6}$$

2.4.3 Measuring point layout of reinforcement and concrete strain

The resistance strain gauge was used to measure the strain on the surfaces of longitudinal reinforcement, stirrup, and concrete. The strain gauge for reinforcement had a type of BX120-3AA, a resistance value of 119.9 ± 0.1 Ω, a sensitivity coefficient of 2.08 ± 1%, and a gate dimension of 5 mm × 3 mm. The strain gauge for concrete had the same type, resistance type, sensitivity coefficient as that for reinforcement, but a different gate dimension of 100 mm ×3 mm.

The measuring points of the longitudinal reinforcement and stirrup strain were mainly arranged via the reinforcement of the plastic hinge region at the bottom of the bridge column. The strain gauges for longitudinal reinforcement were arranged on the four faces of the column at positions corresponding to 50, 200, 400, 600, and 1,200 mm above the bottom of the column. The strain gauges for the stirrup were arranged on the four faces of the column at positions corresponding to 50, 100, 200, 300, and 400 mm above the bottom of the column. Figures 7–9 show the measuring point layout of reinforcement and concrete strain.

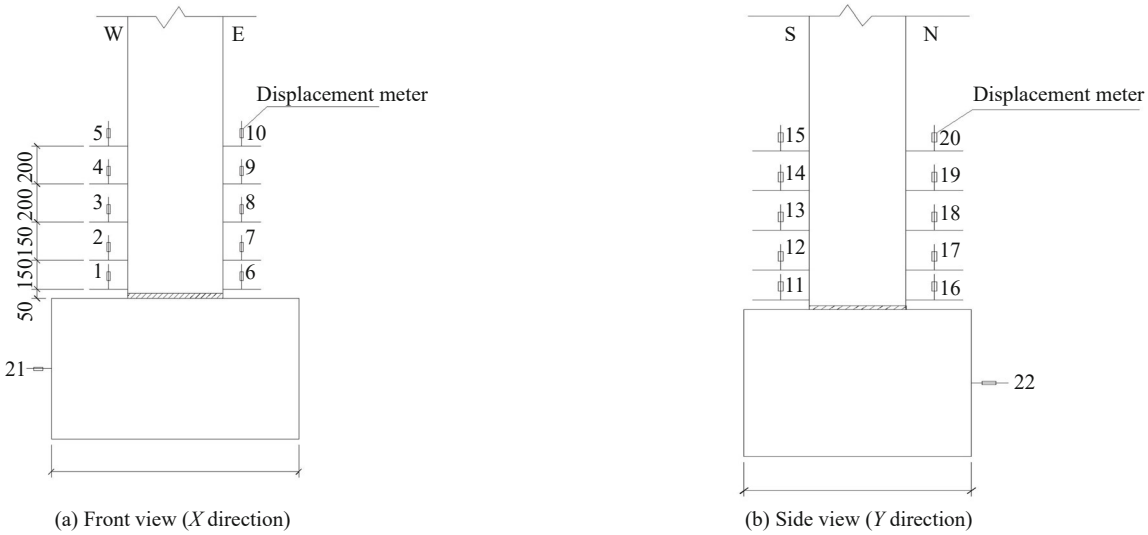

(a) Front view (*X* direction) (b) Side view (*Y* direction)

Fig. 6 Displacement sensor layout (mm)

Table 5 Displacement measuring point layout of the specimens

Specimen No.	Displacement at the top of the bridge column	Sliding displacement of the pile cap	Opening-closing extent at joints
RC0, BBPC-1–BBPC-4	Electro-hydraulic servo loading system	21, 22	1, 6, 11, 16

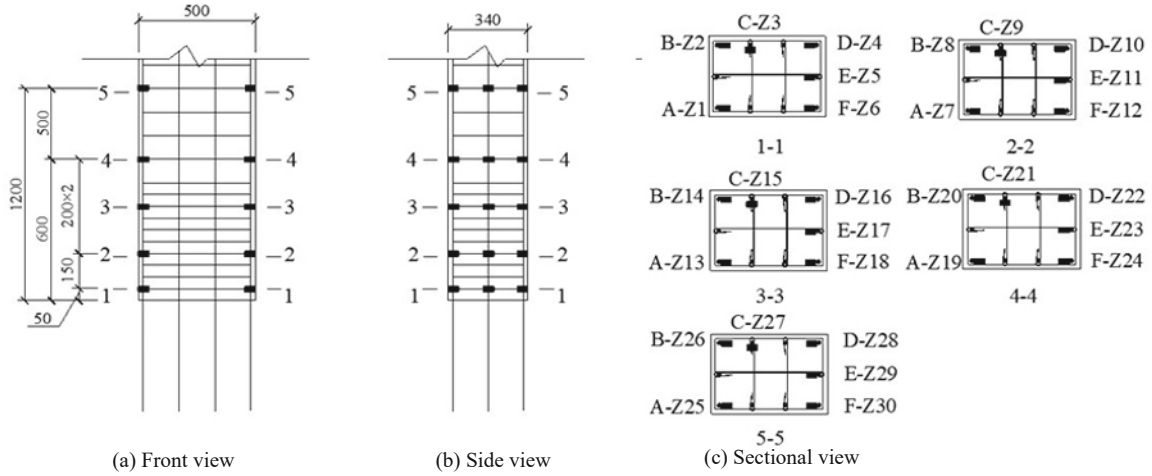

(a) Front view (b) Side view (c) Sectional view

Fig. 7 Strain gauge layout of longitudinal reinforcement

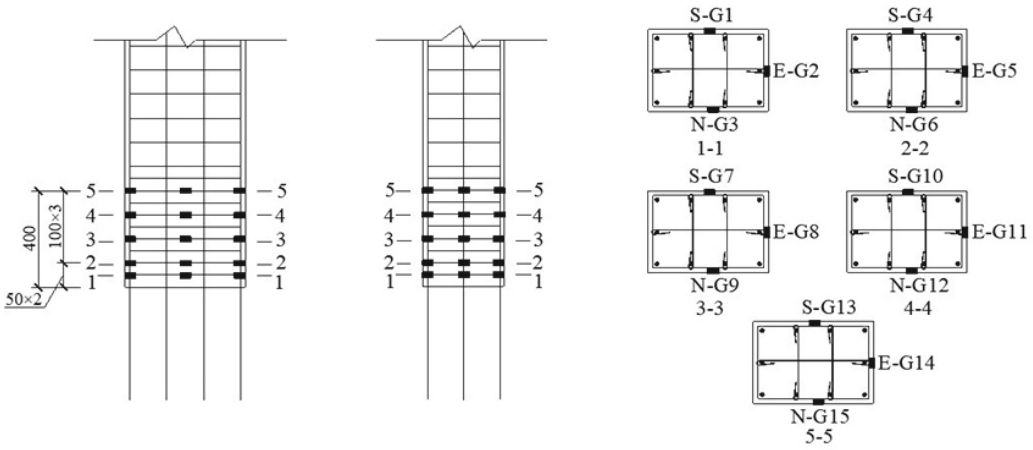

(a) Front view (b) Side view (c) Sectional view

Fig. 8 Strain gauge layout of stirrups

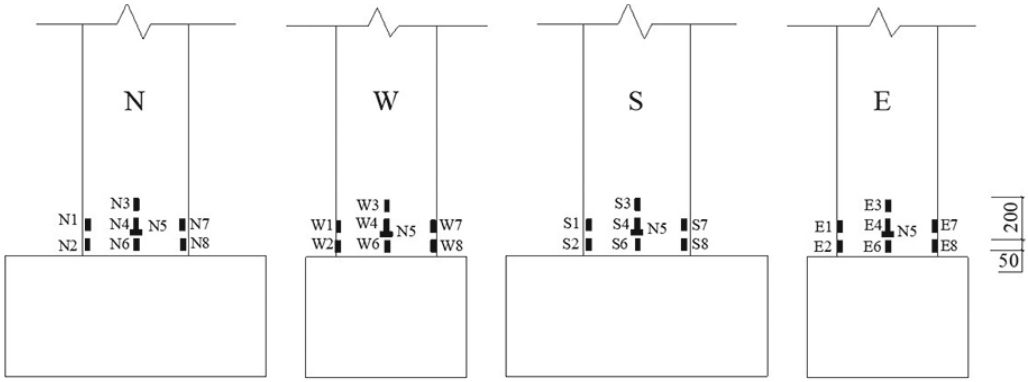

Fig. 9 Strain gauge layout of the four surfaces

3 Experimental results and discussion

3.1 Damage characteristics

The damage development process of the five specimens was observed and compared: it involved concrete cracking, reinforcement bar yielding, concrete crushing, and reinforcement buckling. As expected, the results show that the damage process of the five different precast bridge column specimens was similar, starting from the surface-concrete cracking at the bottom of the bridge column (Fig. 10(a)) to the yielding of the longitudinal reinforcement (Fig. 10(b)). Then, the concrete cover spalled and crushed (Fig. 10(c)), and finally the longitudinal reinforcement buckled. The difference was that the concrete cracking of the precast bridge columns connected with GCMD was accompanied by the phenomenon of the joint opening, which may lead to a reduction in initial stiffness. This observation is consistent with other studies on reinforced concrete bridge columns, such as Lehman *et al*. (Lehman *et al.*, 2004). As suggested by Lehman *et al.* (2004), concrete cover spalling and crushing of the concrete core were damage states that require repair or significant repair. After the test, the longitudinal reinforcement bars embedded in the GCMD were not pulled out, indicating that GCMD performs well in connecting the column and footing under bi-directional lateral load.

The final damage states of the five specimens are shown in Fig. 11. As can be seen from the figures, all specimens were subjected to classic flexural failure, which involved concrete crushing and longitudinal steel bar buckling. Note that the longitudinal bars in the plastic hinge region of the BBPC-2 and BBPC-3 specimens were observed to be fractured after the test took place.

To further illustrate the damage states of the bridge columns, the crack distribution and the damage position of each specimen were measured and drawn, as shown in Fig. 12, where the black area at the bottom represents the crushed concrete. Some meaningful results were found as follows:

(1) The BBPC-2 (precast) and RC0 (cast-in-place) specimens had almost the same concrete cracking height and the concrete crushing scope in the plastic hinge region, which means these two specimens would have a similar seismic performance.

(2) The bi-directionally loaded BBPC-2 specimen had a larger crack distribution height and suffered more several damage when compared to the uni-directionally loaded BBPC-1 specimen, which indicates the bi-

(a) (b) (c)

Fig. 10 Typical damage stages: (a) surface-concrete cracking; (b) longitudinal reinforcement yielding; (c) concrete spalling and crushing

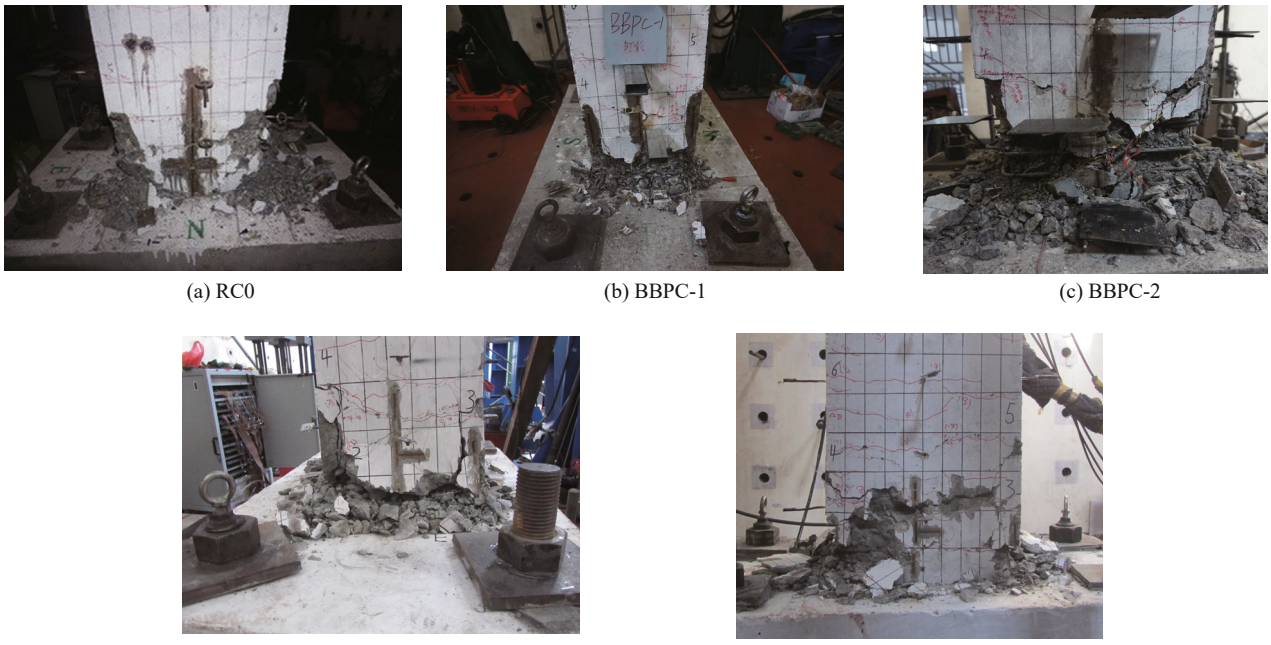

(a) RC0 (b) BBPC-1 (c) BBPC-2

(d) BBPC-3 (e) BBPC-4

Fig. 11 Final failure states of the CIP bridge column (RC0) and precast bridge columns with GCMD (BBPC-1 to 4)

directional load leads to more severe damage to a precast bridge column compared to a uni-directional load.

(3) Three specimens BBPC-3, BBPC-2 and BBPC-4 with the same axial load ratio had different slenderness ratios, namely, 4.12, 7.06 and 10, respectively. As shown in Fig. 12, the final crack distribution height for the three specimens was 85, 133, and 200 cm, respectively, indicating that the specimens that exhibit a larger slenderness ratio have a higher crack distribution. However, the concrete crushing degree of BBPC-3 was obviously less than that of BBPC-2 and BBPC-4, which is attributed to the smaller slenderness ratio of BBPC-3 and the more concentrated deformation at the connection, resulting in a larger deformation of the reinforcement bars and a lesser degree of crushing of the concrete. This indicates that the reinforcement bars of BBPC-3 will yield, buckle or fracture earlier in the test, which was also verified by the failure mode and the smallest ultimate drift ratio of BBPC3 among the three specimens, BBPC-3, BBPC-2 and BBPC-4.

3.2 Seismic performance analysis and comparison

To understand the seismic performance of the precast bridge column, the five specimens were then experimentally investigated by considering the influence of production method, loading pattern, and slenderness ratio. Through the analysis of the hysteresis loop, skeleton curve, and displacement ductility of the five specimens, six seismic indexes were evaluated in this study, including energy dissipation, residual displacement, ultimate load, drift ratio, ultimate displacement, and displacement ductility, etc.

The hysteresis loop could present the hysteresis characteristics of the specimens, including energy dissipation, residual displacement, and stiffness degradation. Generally, the fuller the hysteresis loop is, the better the seismic performance (Xu *et al.*, 2017). Regarding the skeleton curve, it is the line connecting the peak of the first hysteresis loop in each loading displacement that can show the ultimate load, ultimate

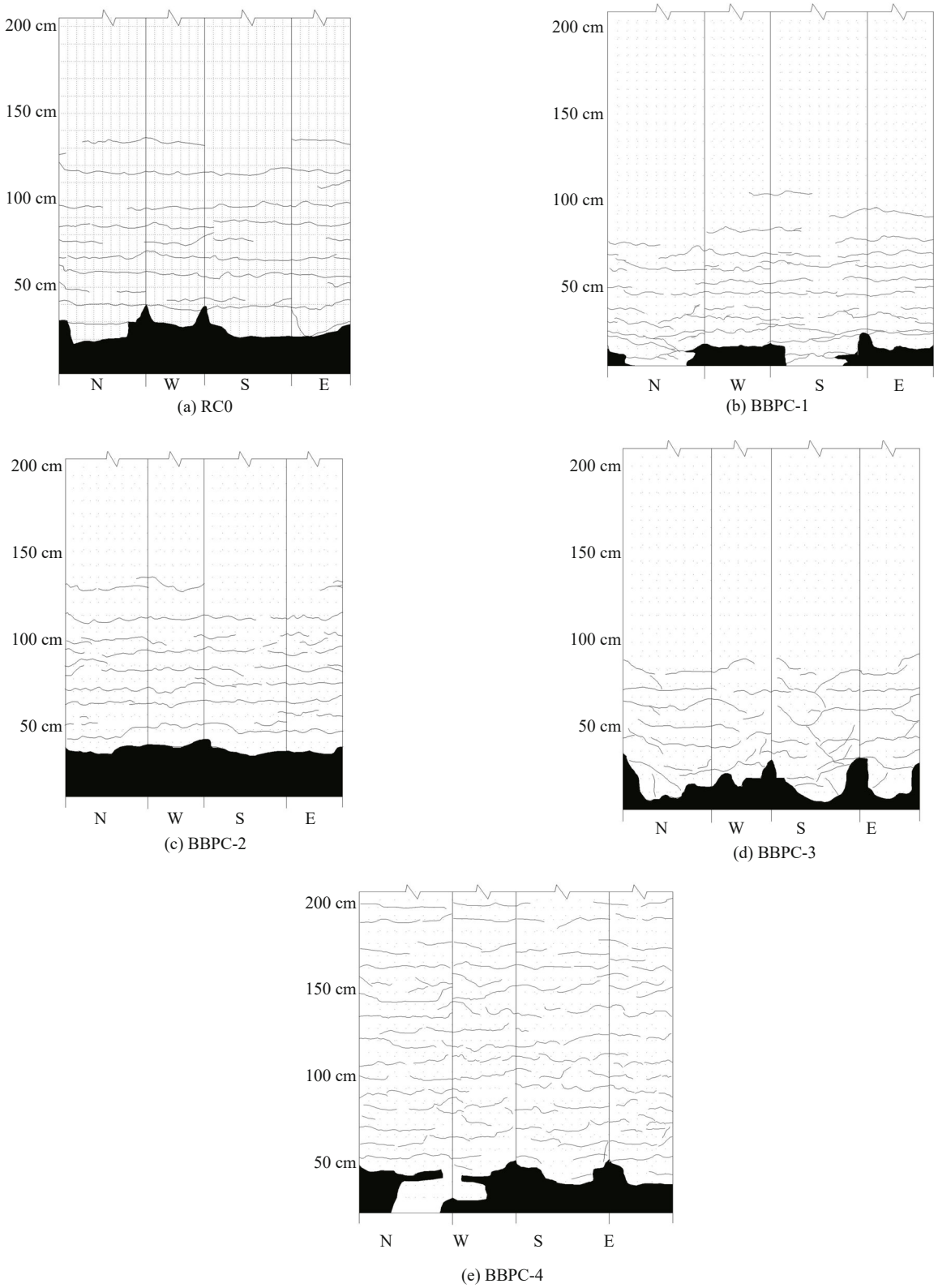

Fig. 12 Comparison of the final failure mode of the CIP bridge column (RC0) and precast bridge columns with GCMD (BBPC-1 to 4)

displacement, drift ratio, and strength degradation, etc. (Xu *et al.*, 2017). Ultimate displacement was defined as the displacement when the load dropped to 85% of its ultimate load.

3.2.1 Comparison between RC0 and BBPC-2

A comparison of the CIP specimen RC0 and the precast specimen BBPC-2 (see Figs. 13(a) and 13(b))

shows that in *X* and *Y* directions, the hysteresis loops of the two specimens were both full and matched well. The hysteresis dissipated energies were close to each other in both *X* and *Y* directions, as shown in Figs. 13(c) and 13(d). Also, hysteresis dissipated energy increased significantly when the drift ratio became larger at the later loading stage. The residual deformation of RC0 and BBPC-2 were also similar (see Figs. 13(e) and 13(f)). Thus, both the CIP and precast specimens had a similar and good energy dissipation capacity, which indicates that the designed precast segmental specimen has the same hysteresis characteristics as the CIP specimen, and achieves the expected target performance.

Figure 14 shows the comparison of the skeleton curves of the CIP specimen RC0 and the precast specimen BBPC-2. Consistent with the hysteresis loop, skeleton curves of the two specimens also matched well, and the ultimate load, ultimate displacements and drift ratio

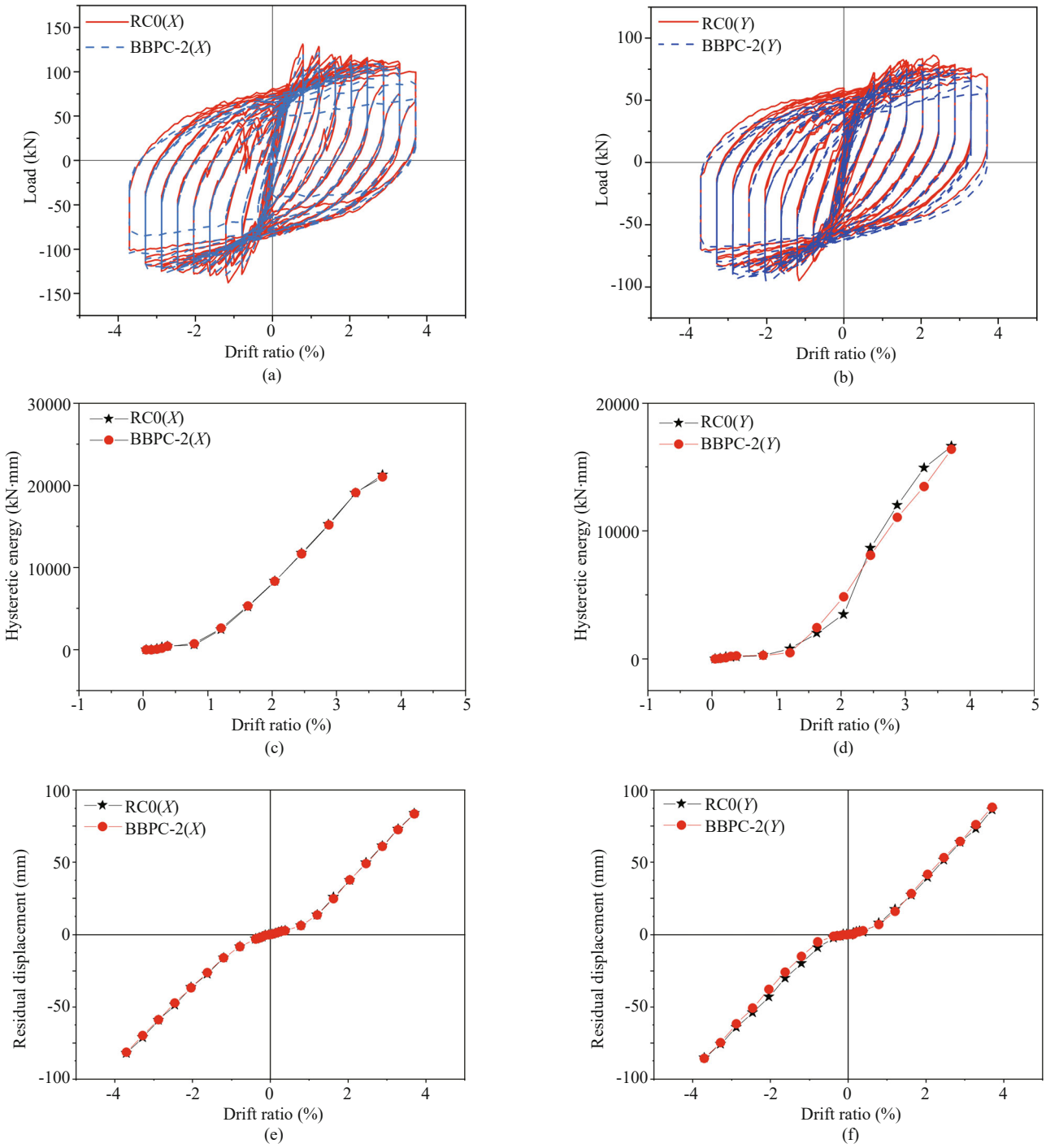

Fig. 13 Comparison of the hysteresis loops between the CIP bridge column and the precast bridge column in (a) *X* and (b) *Y* directions, the hysteresis energy values in (c) *X* and (d) *Y* directions, the residual displacements in (e) *X* and (f) *Y* directions

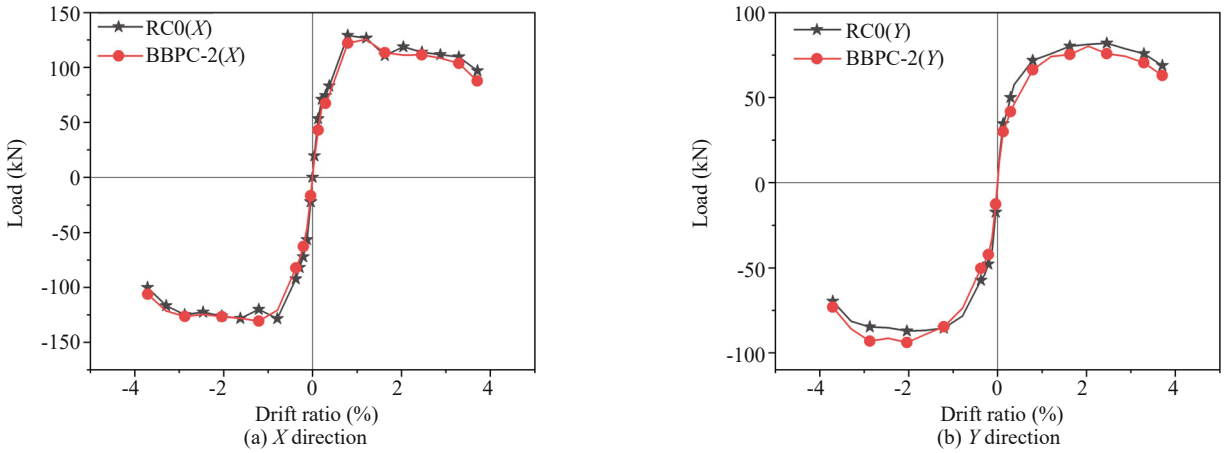

Fig. 14 Comparison of the skeleton curves of bi-directionally loaded specimens

were relatively close. Combined with the comparison of the hysteresis loops, it can be concluded that the seismic performance of the precast specimens connected with GCMD is close to that of the CIP bridge columns under the bi-directional load, achieving the design goal of performance equivalence.

Park method (Park, 1989) was used to calculate the yield displacement and yield load of the tested specimens (see Fig. 15). The ductility coefficient μ is expressed as

$$\mu = \frac{\Delta_u}{\Delta_y} \tag{7}$$

where Δ_u is the ultimate displacement, defined as the corresponding displacement when the load drops to 85% of the maximum load; Δ_y is the yield displacement, which was determined by Park method.

Due to the opening phenomenon of the precast specimen connected with GCMD, the initial stiffness at the initial loading stage was slightly smaller than that of the CIP specimen, resulting in a larger yield displacement. Therefore, the displacement ductility of the BBPC-2 specimen in *X* and *Y* directions were 12% and 15%, that is, smaller than those of the RC0 specimen (see Table 6). In Table 6, the measured feature values, e.g., the load and displacement values shown in the table, are the average values in *X* and *Y* directions.

3.2.2 Comparison between BBPC-1 and BBPC-2

Figure 16(a) shows the hysteresis curves of the BBPC-1 and BBPC-2 specimens in *X* direction. It can be seen from the figure that, compared to the hysteresis curve of the BBPC-2 specimen under a bi-direction load, the hysteresis area of the hysteresis curve of the BBPC-1 specimen under uni-directional load was larger, which indicates that the BBPC-1 specimen has a larger energy dissipation capacity in *X* direction (see Fig. 16(b)). At the same time, it was found that the hysteresis loop of BBPC-2 was flatter, and the strength degradation and the unloading stiffness were larger. This means that the

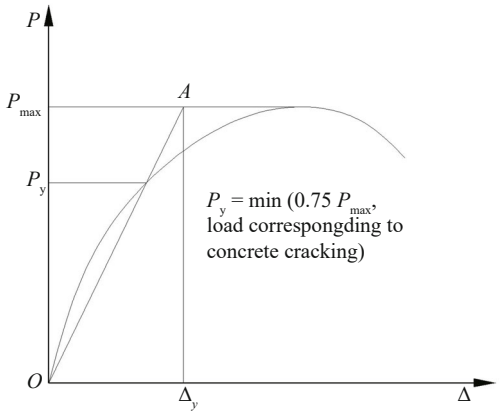

Fig. 15 Park method to determine yield strength and displacement

BBPC-2 specimen suffered more severe damage, which was in accordance with the failure process of the tested specimens. In the unloading stage, the hysteresis curve of the BBPC-2 specimen showed an inverted Z shape due to the buckling and fracture of steel bars. Due to the large unloading stiffness of the precast bridge column connected with GCMD under a bi-direction load, the residual displacement of the BBPC-2 specimen was also significantly larger than that of the BBPC-1 specimen (see Fig. 16(c)). The test results show that the bi-directional loading action would aggravate the damage of the precast bridge column in the plastic hinge region (see Figs. 12(b)–12(c)) and would lead to the worst hysteresis performance when compared with the precast bridge column under a uni-directional load.

Figure 16(d) shows the load-drift ratio skeleton curves of the BBPC-1 and BBPC-2 specimens in *X* direction. It can be seen from the figure that the ultimate load (127.3 kN) and displacement drift ratio (3.39%) of the BBPC-2 specimen under the bi-directional load were 11.8% and 18.4% lower than those of the BBPC-1 specimen under the uni-directional load. This result can also be observed in Fig. 16(a). Combined with

Table 6 Characteristics of the specimens in load, displacement, ductility, and drift ratio

Specimen No.		Yield displacement Δ_y (mm)	Yield load P_y (kN)	Peak load P_{MAX} (kN)	Ultimate displacement Δ_u (mm)	85% Peak load	Ductility coefficient (Park method)	Displacement drift ratio (%)
RC0	*X*	14.8	111.9	128.8	80.7	109.5	5.45	3.36
	Y	16.3	70.7	81.6	86.5	69.4	5.31	3.60
BBPC-1	*X*	17.0	125.5	147.6	96.9	125.5	5.70	4.04
BBPC-2	*X*	16.5	114.9	128.1	79.2	108.9	4.80	3.39
	Y	18.3	73.4	87.1	82.9	74.0	4.53	3.45
BBPC-3	*X*	12.2	195.2	231.7	37.4	196.9	3.07	2.67
	Y	11.1	112.9	128.6	50.0	109.3	4.50	3.57
BBPC-4	*X*	28.5	73.1	81.6	127.0	69.4	4.46	3.74
	Y	33.0	39.9	48.6	127.0	41.3	3.85	3.74

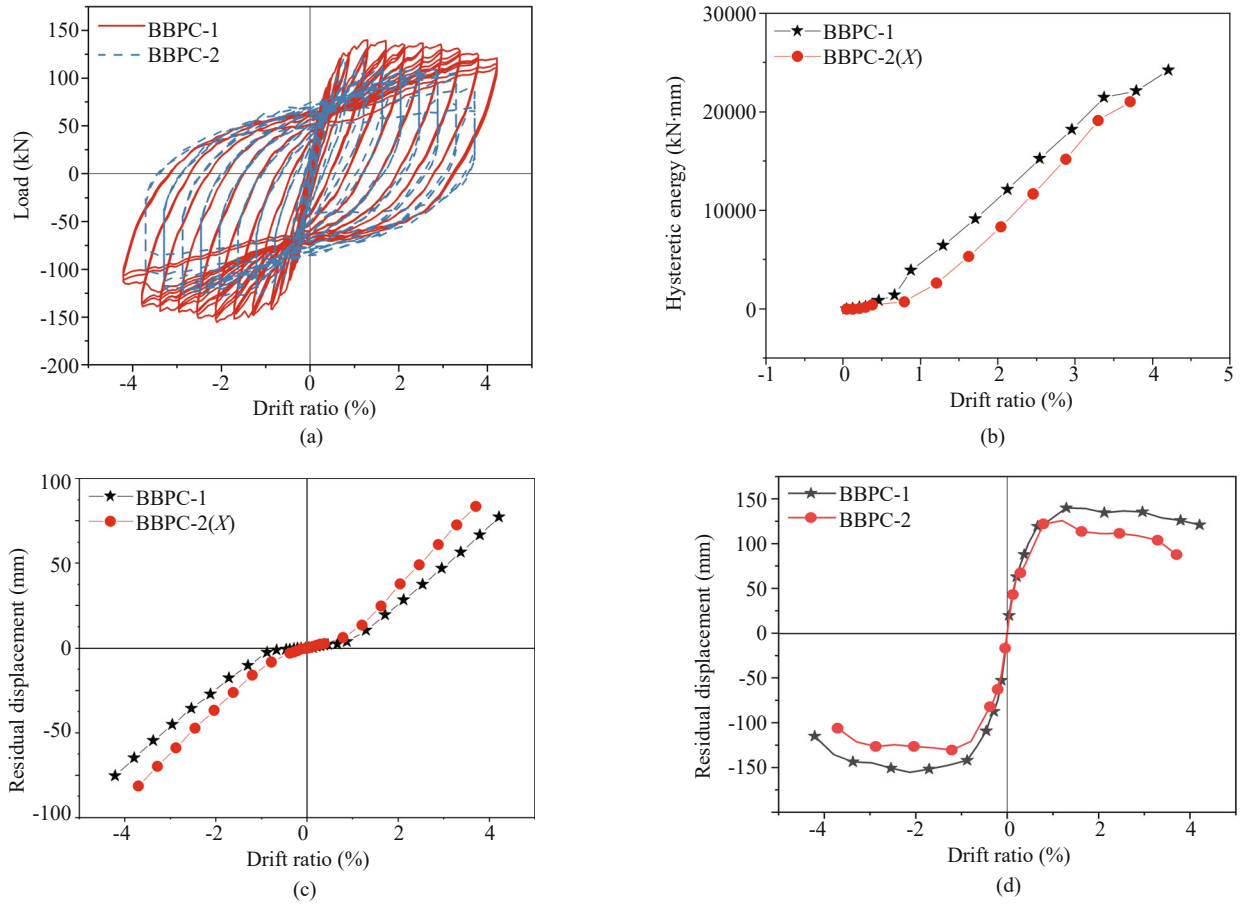

Fig. 16 Comparison of seismic performance of the specimens under uni-directionally and bi-directional loads: (a) the hysteresis loops and (b) its hysteresis energy (c) residual deformations and (d) skeleton curves

the comparison of the energy dissipation capacity and residual deformation (see Figs. 16(b) and 16(c)), it can be seen that the bi-directional load has a disadvantageous impact on the seismic performance of precast bridge columns, resulting in a significant decrease of the energy dissipation capacity, ultimate bearing capacity and ultimate drift ratio, etc. Table 6 also shows that the displacement ductility (5.70) of the BBPC-1 specimen was 19.0% greater than that of the BBPC-2 specimen (4.80), indicating that the bi-directional load also reduces the displacement ductility of precast bridge columns. Therefore, the influence of the bi-directional load should be urgently considered in the seismic design of precast bridge columns connected with GCMD.

3.2.3 Influence of slenderness ratio

The influence of the slenderness ratio on the hysteresis loops and hysteresis dissipated energy was then compared and analyzed (see Fig. 17). The three specimens, BBPC-

3, BBPC-2 and BBPC-4, had the same axial load ratio (i.e., 0.1) but with different slenderness ratios (i.e., 4.12, 7.06 and 10.00). This demonstrates that regardless of either *X* or *Y* direction, the larger the slenderness ratio, the flatter the hysteresis loop and the smaller hysteresis area would be, and, the faster that its strength would degrade (see Figs. 17(a)–17(b)). However, it is meaningful to note that when the drift ratio at the top of the bridge column was only 2.67, the BBPC-3 specimen with the smallest slenderness ratio among the three specimens failed. Its energy dissipation capacity began to drop rapidly, resulting in the accumulative energy being smaller than that of the BBPC-2 and BBPC-4 specimens (see Figs. 17(c)–17(d)), which indicates that an insufficiently low slenderness ratio is not conducive to the energy dissipation of a precast bridge column. With the proper slenderness ratios (7.06 and 10.0), the precast bridge columns BBPC-2 and BBPC-4 can obtain a better seismic performance when compared to the BBPC-3 specimen, including a larger energy dissipation capacity, a larger drift ratio and a correspondingly smaller residual displacement (see Figs. 17(e)–17(f)).

The influence of slenderness ratios on the skeleton curves was also examined. Figure 17 shows that regardless of *X* or *Y* direction, the smaller the slenderness ratio of the specimen, the larger the peak load and the ultimate load; however, the faster the load decreased, the lower the deformation capacity of the specimen. This

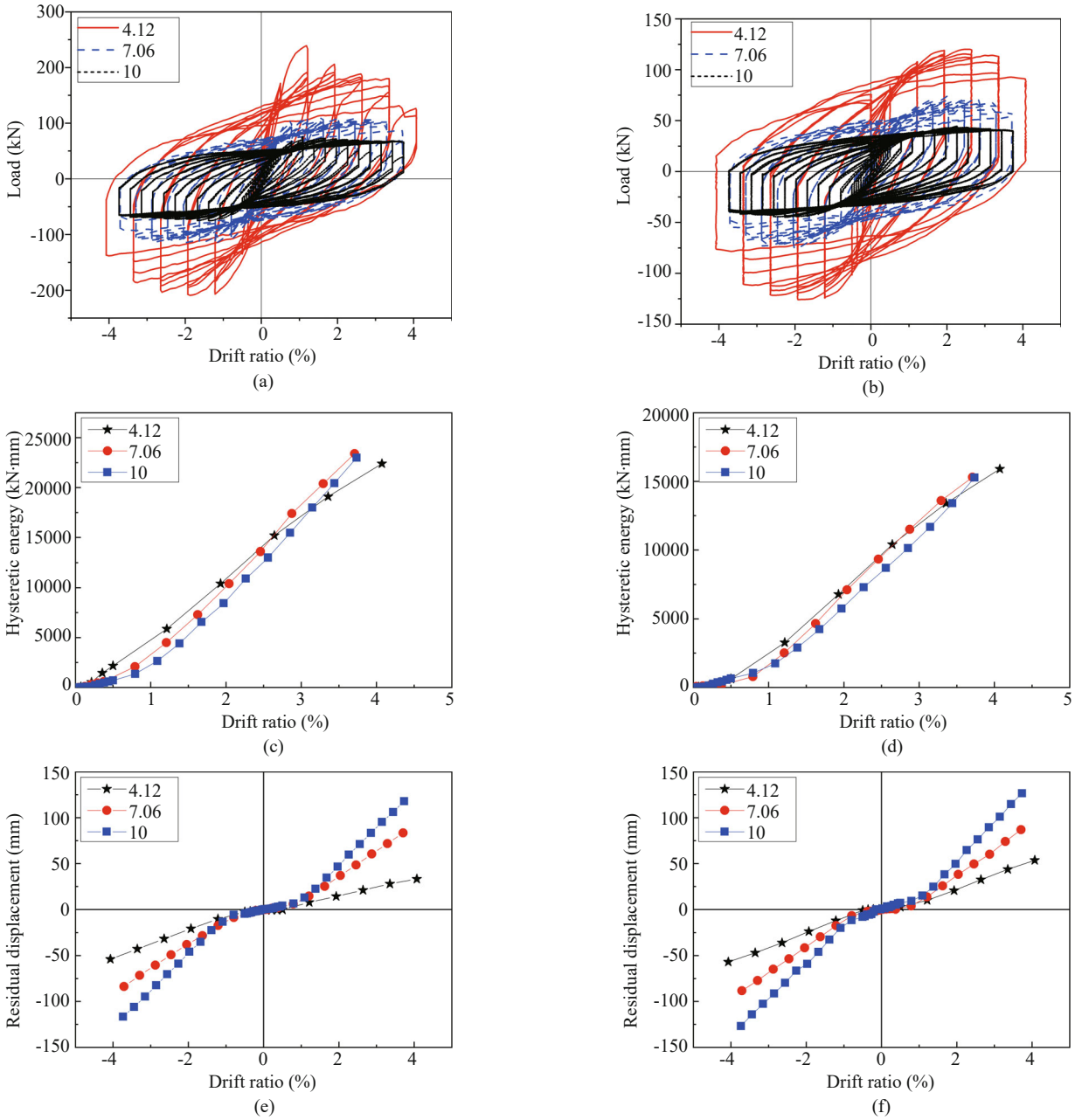

Fig. 17 Comparison of the hysteresis loops of different slenderness ratio specimens in (a) *X* and (b) *Y* directions, the corresponding hysteresis energy values in (c) *X* and (d) *Y* directions, and the residual deformations in (e) *X* and (f) *Y* directions

observation matches well with the previous laboratory test or numerical results (e.g., Peng *et al.*, 2018). It also can be seen from Table 6 that the maximum drift ratios of the BBPC-3, BBPC-2 and BBPC-4 specimens were 2.67%, 3.39% and 3.74%, respectively (with the maximum drift ratio of each specimen taking the smaller value in the two directions), indicating that there is no linear relationship between the slenderness ratio and the drift ratio for the tested specimens. The maximum drift ratio of the BBPC-3 specimen was significantly smaller that of the BBPC-2 and BBPC-4 specimens. This is mainly because there was no stirrup constraint at the connection joint of the precast bridge columns connected with GCMD. When the slenderness ratio was too small, the deformation was more concentrated on the longitudinal reinforcement, which led to premature yield and fracture under the bi-directional load. Therefore, the slenderness ratio of the precast bridge column should not be too small. Similarly, the displacement ductility coefficient (3.07) of the BBPC-3 specimen with a small slenderness ratio was significantly smaller than that of the BBPC-2 and BBPC-4 specimens (4.53 and 3.85, respectively), and the displacement ductility coefficient was also taken as the smaller one in two directions. Therefore, it is suggested that the slenderness ratio of the precast bridge columns connected with GCMD should be 7.0–10.0. Note that the column with a slenderness ratio more than 10.0 is defined as the tall column, whose seismic performance still lacks sufficient research and understanding at present (Wang *et al.*, 2018).

Through the above analysis of seismic performance with regard to hysteresis dissipated energy, residual displacement, skeleton curve, ultimate displacement, and drift ratio, etc., it is found that a reasonably designed precast bridge column connected with GCMD is mainly subjected to the bending failure, and has a similar seismic performance to that of the CIP bridge column.

Generally, a high amount of spending is required to design structures for elastic response due to the consequences of severe earthquakes. Alternatively, engineers prefer to design structures for a lower force level and detail them to produce sufficient energy dissipation capacity to prevent structure collapse (Bae, 2005). This study shows that the hysteresis energy dissipation capacity of the precast bridge column connected with GCMD was similar to the CIP bridge column (see Figs. 13(a)–13(d)). It is noted that the longitudinal reinforcement rebar used has a yield strength of 241 MPa, which is within the normal range of strength. For rebars with what is considered high strength (more than 500 MPa), the energy dissipation of precast bridge column connected with GCMD could be different from that of CIP bridge columns (Zhuo *et al.*, 2018). Future studies needed to be conducted to understand the influence of longitudinal reinforcement on hysteresis energy dissipation capacity.

However, the precast bridge column connected with GCMD under bi-directional load exhibits lower seismic performance than that under uni-directional load. This is consistent with other studies (Li *et al.*, 2018; Marriot *et al.*, 2011). Saatcioglu and Ozcebe (1989) concluded that columns subjected to varying bi-directional loads demonstrate severe strength and stiffness degradation compared to those under uni-directional load. This means that bi-directional load also should be included in the seismic design of the precast bridge column connected with GCMD.

The parameter of slenderness ratio has a significant effect on peak load and hysteresis dissipation capacity of the precast bridge column connected with GCMD. Additionally, the precast bridge column with an appropriate slenderness ratio could have a good seismic performance with respect to a good hysteresis dissipation capacity and deformation capacity. To enhance the understanding of the seismic performance of the precast bridge column connected with GCMD, other parameters such as axial load ratio, longitudinal reinforcement ratio and concrete strength are expected for seismic performance analysis. However, a thorough experiment including the analysis of those parameters is of high cost, leading to numerical simulation in the following section.

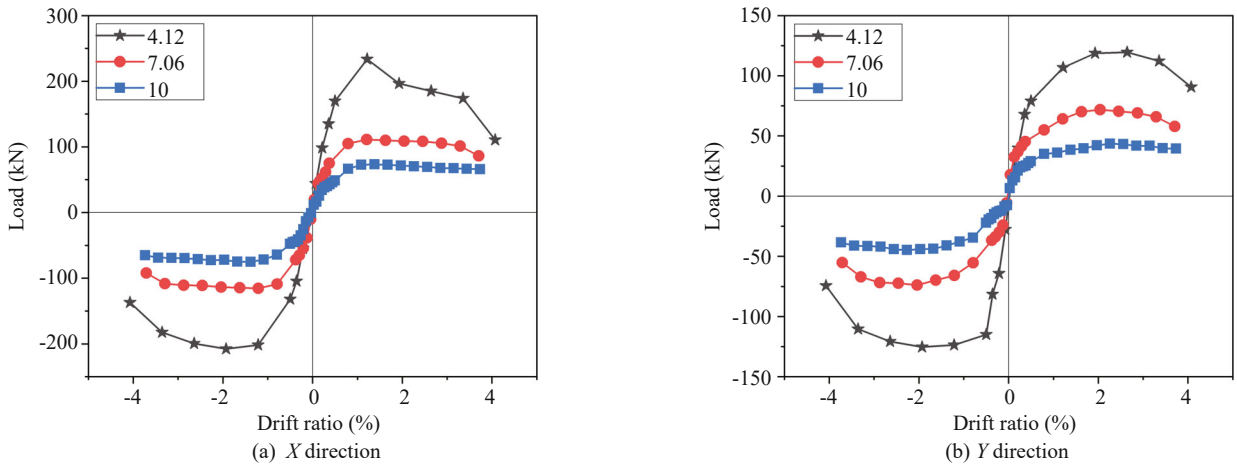

Fig. 18 Comparison of the skeleton curves of specimens with different slenderness ratios

4 Numerical analysis

4.1 Finite element model

4.1.1 Structure model and loading

In this section, a finite element model (FEM) of the precast bridge columns connected with GCMD was established using OpenSees software. There are two types of nonlinear beam-column elements in OpenSees. One consists of nonlinear beam-column elements (Scott *et al.*, 2004) and plastic hinge elements (Scott and Fenves, 2006) based on the compliance theory; the other contains nonlinear beam-column elements based on the stiffness theory. The type of nonlinear beam-column elements based on the flexibility theory was adopted in the FEA model for the purpose of this study. Several studies (e.g., Shooshtari *et al.*, 2015) using nonlinear beam-column elements to examine the nonlinear behaviors of structures in OpenSees software has been reported.

The gravity of the superstructure was simulated by applying the concentrated load on the top of the bridge column. To simplify the model, the weights of the column and the loading head were ignored. The fiber cross-section of the bridge column was divided into three types according to the material characteristics, i.e., unconstrained concrete fiber (cover concrete fiber), core concrete fiber and steel fiber, as shown in Fig. 19.

The parallel springs that were established with zero-length element were applied to simulate the joints, and elastic-perfectly plastic (EPP) material without considering tensile behavior was adopted in the zero-length element. Two types of parallel springs were included in the model to simulate the actual mechanical behavior of the joints. One type of springs (an edge spring), placed at each edge of the section, was used to simulate concrete cracking at the joints. The other type of springs (core spring) that were arranged in the core concrete region was used to simulate the opening and closing phenomena of joints. Thus, the improved Kent-Park model (Concrete02 Model) was adopted for the first type of springs. Elastic-No Tension (ENT) material was applied to the core spring to simulate the mechanical behaviors of core concrete at the joints. The corresponding constitutive model of ENT is shown in Fig. 20, where the measured strength was expressed by using elastic modulus (E), which was set to 15 times that of the cover concrete, ensuring rigid contact of the core concrete on the contact surface without the intrusion of the concrete in the upper and lower parts.

The establishment process of the FEM of CIP columns by using the nonlinear beam-column element was relatively simple. Five elements were divided along the length of the column, and the material properties were assigned to the corresponding fiber, while the bottom of the column was consolidated. The element division and material properties of the precast bridge column were consistent with the CIP column, but the joint simulation was relatively complicated. The simulation of the joint meant that the lower node of the bottom element and the bottom node were respectively connected to a rigid arm, and the rigid arms were connected by spring elements. Among them, the middle 5/6 parts of the section were rigidly contacted by core springs, and the edges were connected by edge springs. The FEM of the precast column is shown in Fig. 21.

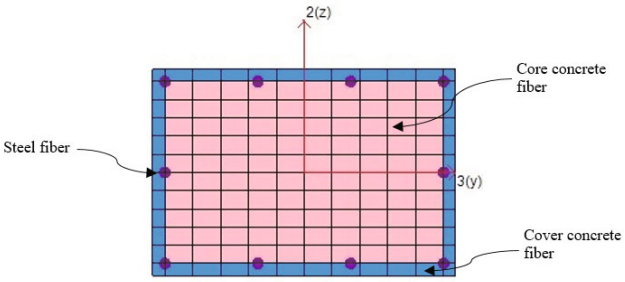

Fig. 19 Fiber cross-section of the bridge column

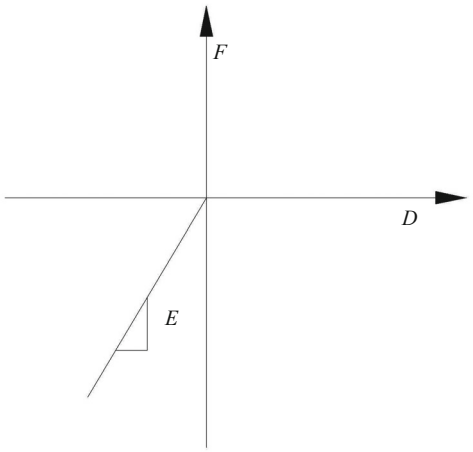

Fig. 20 Rigid contact element

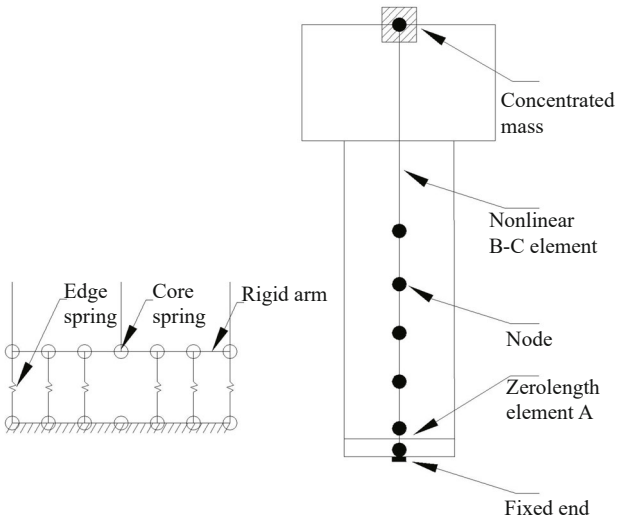

Fig. 21 Finite element model of the precast bridge column

4.1.2 Material models

The improved Kent-Park model (Concrete 02) and the improved Menegotto-Pinto model (Steel 02) were respectively used for the constitutive model of concrete and rebar material (Menegotto and Pinto, 1973; Scott *et al.*, 1982), as shown in Fig. 22.

4.2 Accuracy analysis of the FEM

The developed FEM was calibrated by a comparison of the numerical results and the experimental results regarding the hysteresis loops (both *X* and *Y* directions), which represents the general hysteresis characteristics of all the precast bridge column specimens prepared for this study, i.e., BBPC-1, BBPC-2, BBPC-3, BBPC-4. Figure 22 shows that the calculation hysteresis loops match well with the experimental hysteresis loops.

The FEM calculation results of the hysteresis curves in the *X* and *Y* directions of all the precast bridge columns (i.e., BBPC-1, BBPC-2, BBPC-3, and BBPC-4) were compared with the test results, as shown in Fig. 23. It was found that the calculated hysteresis loops matched well with the test ones, indicating that the FEM displays good accuracy in calculating the hysteresis characteristics. The feature values of the hysteresis curves were also obtained and compared, as listed in Table 7. As can be seen from the table, the testing feature values agree well with the calculating ones.

4.3 Parameter analysis

A parameter analysis was performed to investigate the influence of axial load ratio (5%, 10%, 20%), longitudinal reinforcement ratio (0.90%, 1.18%, 1.50%) and concrete strength (C30, C40, C50) on the seismic performance of the precast bridge columns connected with GCMD.

4.3.1 Axial load ratio

With other parameters being maintained consistently, the axial compression ratios of precast bridge columns connected with GCMD were set to 5%, 10%, and 20%, respectively.

The results from Fig. 24 show that as the axial load ratio increased, the peak load also increased, while the strength dropped sharply, leading to a decrease in the deformation capacity of precast bridge columns. The axial load ratio was found to be insensitive to residual displacement and insensitive to the hysteresis energy in the early loading stage, but the axial load ratio of 10% was obviously beneficial for increasing the hysteresis energy dissipation in the latter loading stage. This result shows that with an increase in the axial load ratio, the ultimate load capacity of the precast bridge column increased, while the deformation capacity decreased, and strength degradation became faster. The comprehensive

Table 7 Comparisons of testing and calculation results

Specimen No.		Yield displacement Δ_y (mm)	Yield load P_y (kN)	Peak load P_{MAX} (kN)	Ultimate displacement Δ_u (mm)
BBPC-1	Testing	17.0	125.5	147.6	96.9
	Calculating	21.2	113.7	129.6	101.0
BBPC-2-X	Testing	16.5	114.9	128.1	79.2
	Calculating	20.7	107.4	106.1	68.4
BBPC-2-Y	Testing	18.3	73.4	87.1	82.9
	Calculating	21.5	62.4	64.4	89.0
BBPC-3-X	Testing	12.2	195.2	231.7	37.4
	Calculating	13.9	191.7	214.1	33.6
BBPC-3-Y	Testing	11.1	112.9	128.6	50.0
	Calculating	13.4	104.2	117.8	51.5
BBPC-4-X	Testing	28.5	73.1	81.6	127.0
	Calculating	30.0	67.9	74.4	116.6
BBPC-4-Y	Testing	33.0	39.9	48.6	127.0
	Calculating	35.2	36.1	42.2	127.0

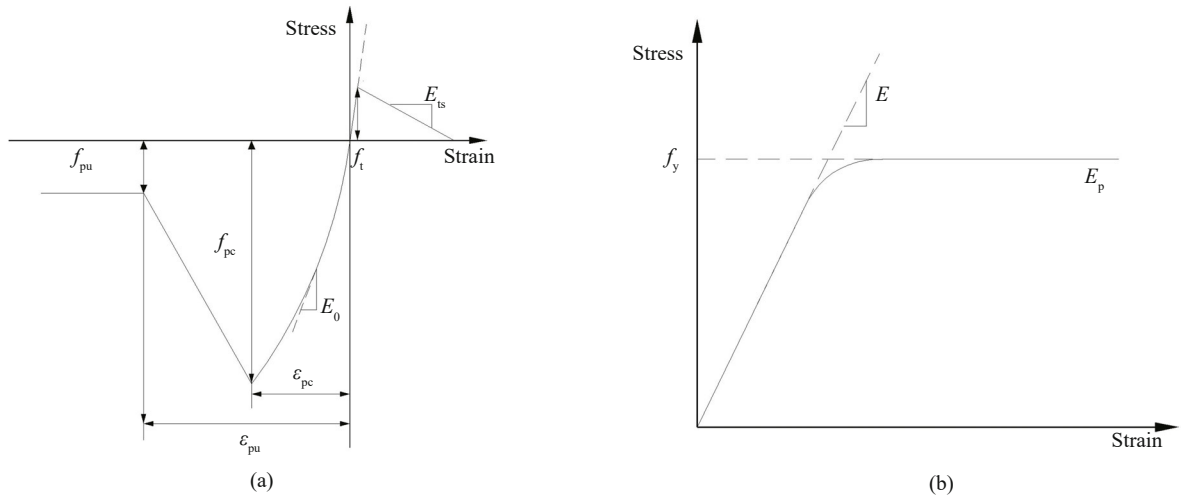

Fig. 22 The constitutive models of (a) Concrete02 and (b) Steel02 in OpenSees

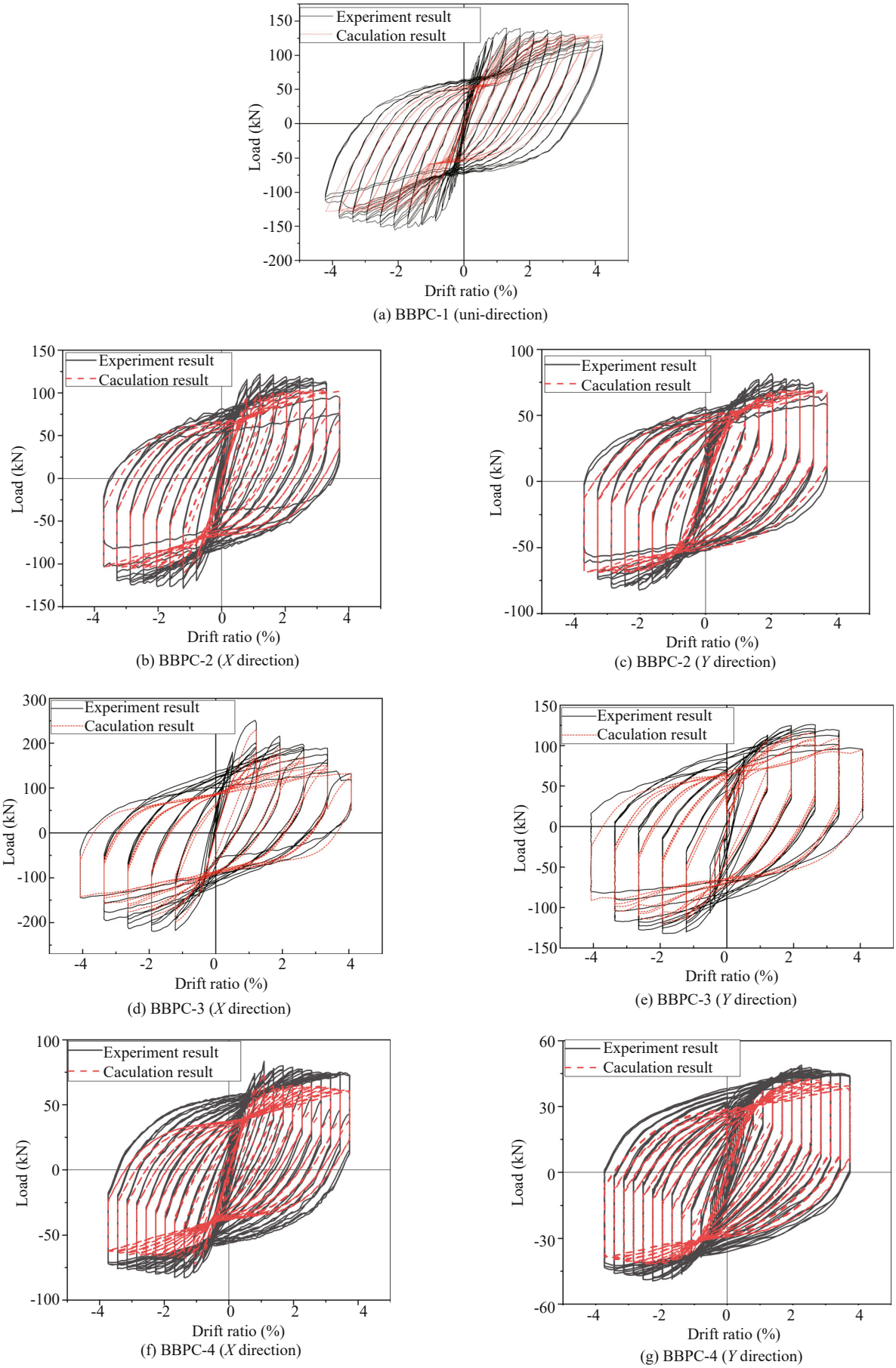

(a) BBPC-1 (uni-direction)

(b) BBPC-2 (*X* direction)

(c) BBPC-2 (*Y* direction)

(d) BBPC-3 (*X* direction)

(e) BBPC-3 (*Y* direction)

(f) BBPC-4 (*X* direction)

(g) BBPC-4 (*Y* direction)

Fig. 23 Comparison of the calculation and experimental results regarding hysteresis curves for all the precast bridge columns, in two directions

analysis indicates that a reasonable axial compression ratio (approximately 10%) is helpful for maintaining a stable strength degradation, as well as obtaining a better deformation capacity and stable energy consumption capacity for the precast bridge columns connected with GCMD.

4.3.2 Longitudinal reinforcement ratio

According to Chinese specifications JTG/T B02-01 (2008) and JTG 3362-2018, the longitudinal reinforcement ratio normally ranges from 0.6% to 4.0%. In this study, the longitudinal reinforcement ratios of the precast bridge columns connected with GCMD were thus set to 0.90%, 1.18%, and 1.50%. Figure 25 shows that with an increase in the longitudinal reinforcement ratio, the peak load was considerably improved, but the variation of residual displacement was negligible. In the early loading stage, the hysteresis dissipated energy of the bridge column with various longitudinal reinforcement ratios was relatively close, but in the later loading stage, the precast bridge column with a higher longitudinal reinforcement ratio demonstrated a better energy dissipation capacity. This can be attributed to the fact that the energy dissipation of the precast bridge column following the joint opening mainly stems from

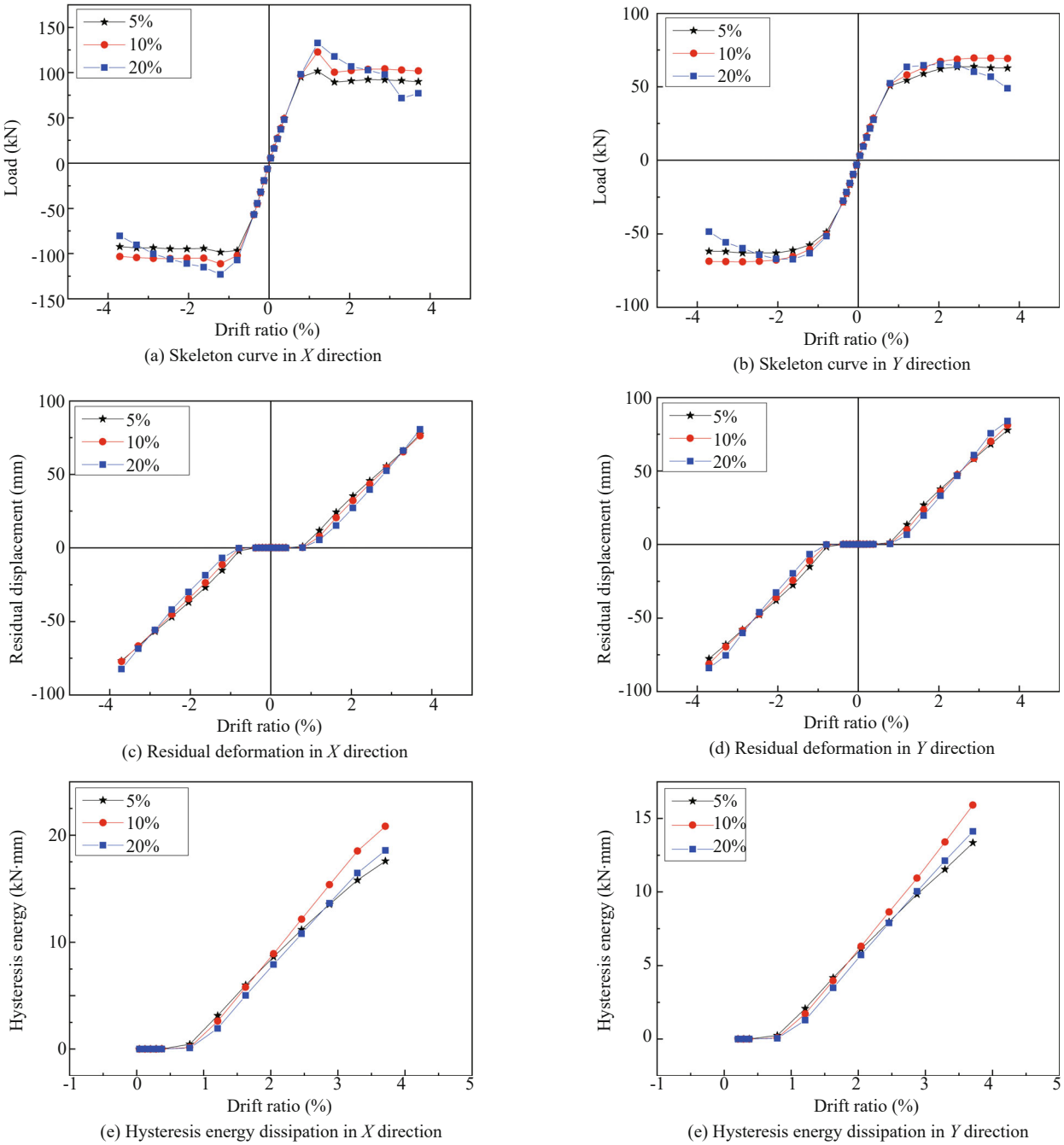

(a) Skeleton curve in *X* direction

(b) Skeleton curve in *Y* direction

(c) Residual deformation in *X* direction

(d) Residual deformation in *Y* direction

(e) Hysteresis energy dissipation in *X* direction

(e) Hysteresis energy dissipation in *Y* direction

Fig. 24 The impact of axial load ratio on the skeleton curve, residual deformation and hysteresis energy dissipation in *X* and *Y* directions

the elastic-plastic deformation of the reinforcement bars. The above observations indicate that the increase in the longitudinal reinforcement ratio can improve the load capacity, the deformation, and the energy dissipation capacities, thereby improving the seismic performance of the precast bridge column.

4.3.3 Concrete strength

Given the importance of bridge safety, the common concrete design strength grades for bridge columns are designed from C30 to C50. Thus, the concrete strengths of the precast bridge columns connected with GCMD were set to C30, C40, and C50. The representative results of the BBPC-2 specimen with variable concrete strength are presented in Fig. 26. This figure shows that concrete strength was insensitive to all investigated seismic indexes, e.g., peak resistance, ultimate load capacity, residual displacement, and hysteresis energy, etc. Therefore, within a range of reasonable design strength (e.g., C30, C40, and C50), the concrete strength has little influence on the mechanical behavior of the connection and the seismic performance of the precast bridge column connected with GCMD.

Although the above experimental and numerical analysis enhance the understanding of the seismic

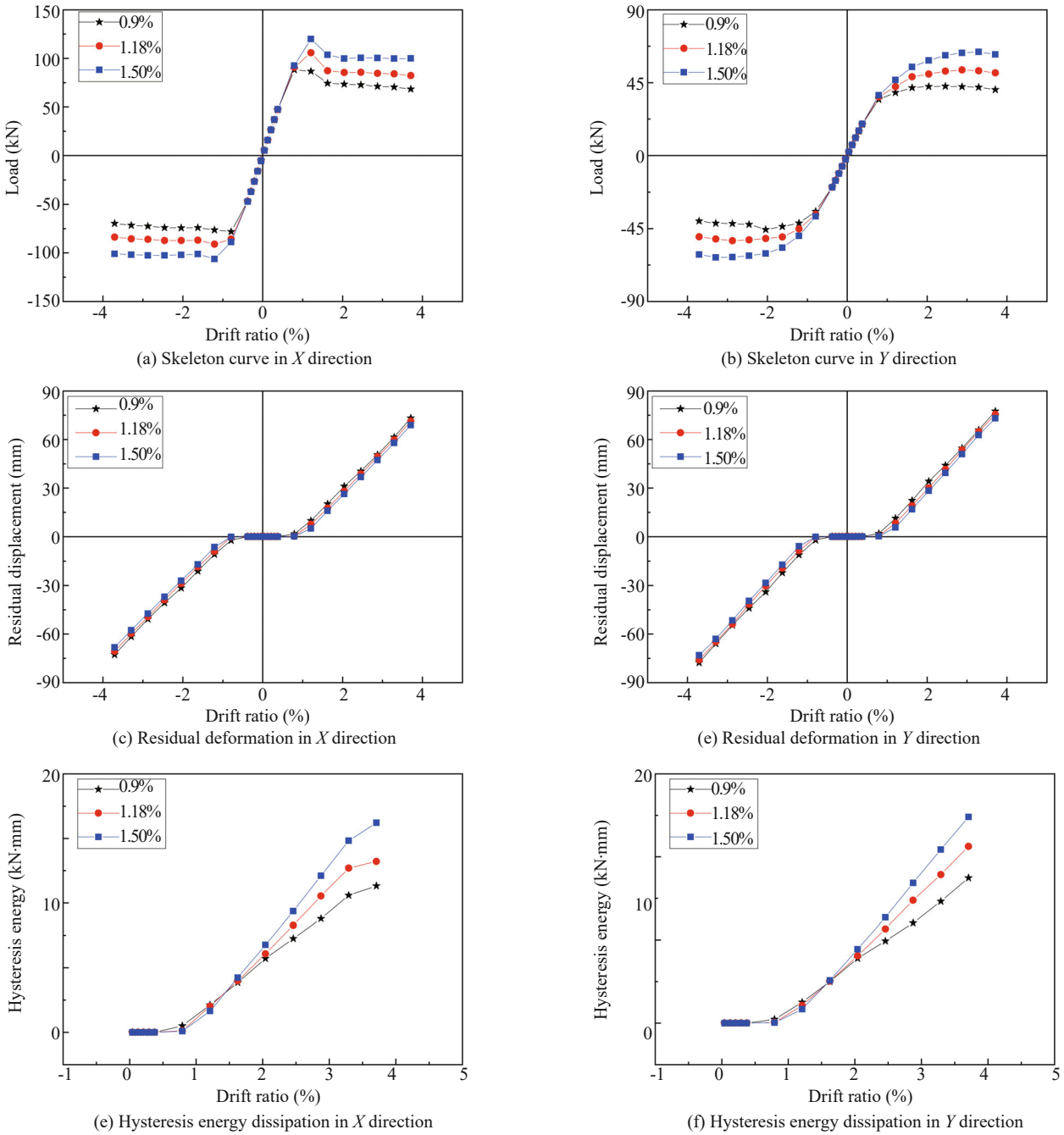

(a) Skeleton curve in *X* direction

(b) Skeleton curve in *Y* direction

(c) Residual deformation in *X* direction

(e) Residual deformation in *Y* direction

(e) Hysteresis energy dissipation in *X* direction

(f) Hysteresis energy dissipation in *Y* direction

Fig. 25 The impact of longitudinal reinforcement ratio on the skeleton curve, residual deformation and hysteresis energy dissipation in *X* and *Y* directions

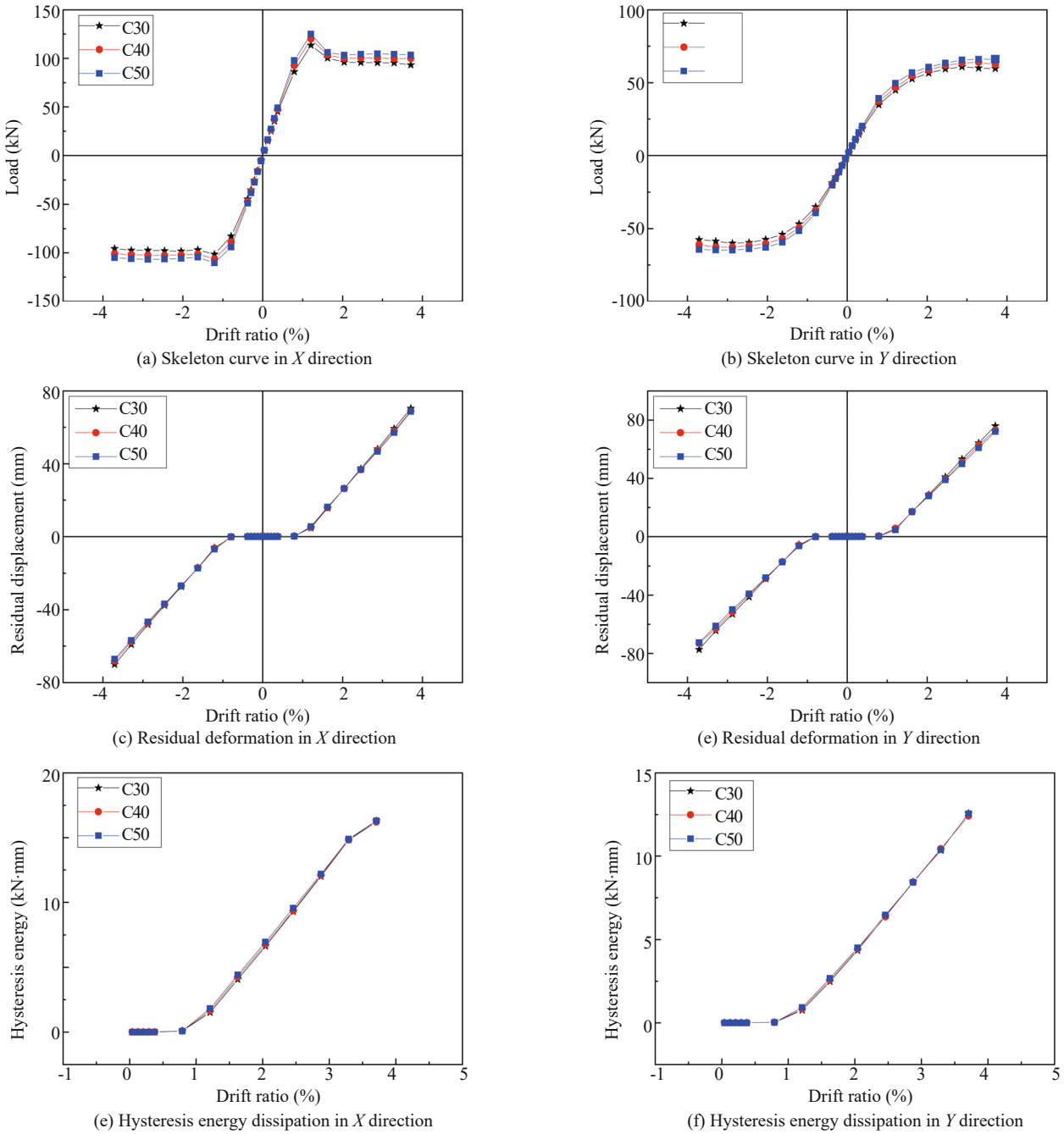

(a) Skeleton curve in *X* direction

(b) Skeleton curve in *Y* direction

(c) Residual deformation in *X* direction

(e) Residual deformation in *Y* direction

(e) Hysteresis energy dissipation in *X* direction

(f) Hysteresis energy dissipation in *Y* direction

Fig. 26 The impact of concrete strength on the skeleton curve, residual deformation, and hysteresis energy dissipation in *X* and *Y* directions

performance of the precast column connected with GCMD, a comprehensive investigation is still needed, particularly the full-scale test. Note that tests on large-scale concrete columns have rarely been conducted (Bae, 2005) and so far, no full-scale test has been reported on the precast column connected with GCMD.

5 Conclusions

In this paper, the seismic performance of the precast bridge column connected with GCMD was compared to that of the CIP column under the bi-directional load. Also, the influence of the uni-direction and bi-direction load, axial load ratio, slenderness ratio, concrete strength and longitudinal reinforcement ratio on its seismic performance was analyzed by experiments and FEA with a parameter analysis. The main conclusions were extracted and listed as follows:

(1) Similar to the CIP bridge column, the precast bridge columns connected with GCMD were mainly subjected to bending failure involving concrete crushing and reinforcement bar buckling under bi-directional load. The difference was that the concrete cracking of the precast bridge columns connected with GCMD was accompanied by the phenomenon of the connection joint

opening, which leads to a concentrated deformation at the connection, resulting in a larger deformation and earlier buckling or fracturing of the reinforcement bars of the precast specimens that have smaller slenderness. This feature was obviously found in the specimen BBPC-3 with a slenderness ratio of 4.12 in the test.

(2) During the test, the precast bridge column under the bi-directional load suffered more significant damage, including an increase in the concrete crushing degree and scope and fracture of reinforcement bars, which results in the decrease of the peak load, ultimate drift ratio and displacement ductility coefficient by 11.8%, 18.4%, and 15.7%, respectively, compared with the test specimen under solely the uni-directional load. This indicates that the bi-directional load has a disadvantageous impact on the seismic performance of the precast bridge columns. Therefore, the action of the bi-directional load should be eagerly involved in the seismic design of the precast bridge columns connected with GCMD.

(3) The hysteresis curves and skeleton curves of the CIP and precast bridge column with the same design parameters were essentially similar in terms of overall performance, including hysteresis dissipated energy, peak load, displacement drift ratio and residual displacement, etc., which means that the precast bridge columns can be designed for an equivalent seismic performance of the CIP bridge column. This also indicates that the GCMD performs well in connecting the column with the footing. However, the displacement ductility coefficient of the precast bridge column was slightly smaller than that of the CIP bridge column. This can be attributed to the joint opening phenomenon in the loading process of the precast bridge column and the corresponding decrease in the initial stiffness, coupled with an increase in yield displacement.

(4) Similar to the CIP bridge column, the slenderness ratio is an important factor that affects the seismic performance of the precast bridge columns connected with GCMD. The precast bridge column with a larger slenderness ratio (e.g., 7.06 and 10.0) can obtain a better seismic performance and is more conducive to resisting the seismic load. Conversely, the decrease in the slenderness ratio will significantly reduce the seismic performance, including the more rapid degradation of strength, the reduction of energy dissipation capacity and deformation capacity, e.g., the maximum drift ratio of the test specimen with a slenderness ratio of 4.12 was only 2.67%. The main reason for this is that when the slenderness ratio is too small, the deformation of the column following the opening of the joint is concentrated in the longitudinal reinforcement, which leads to premature buckling and fractures. Thus, the slenderness ratio of the precast bridge column should not be too small. The primary recommendation of the slenderness ratio for the precast bridge columns connected is 7.0–10.0.

(5) The FEA results show that with an increase in axial load ratio, the ultimate load capacity of the precast bridge column increased, the deformation capacity was reduced, and the energy dissipation capacity was insignificantly improved. An extremely large axial compression ratio will lead to the rapid degradation of strength and a decrease in seismic performance; therefore, an axial compression ratio near 1.0 in the seismic design of the assembled pier is recommended. With the increase in the longitudinal reinforcement ratio, the hysteresis energy dissipation capacity increased, and ultimate load capacity and deformation capacity were significantly improved; thus, the seismic performance of the bridge column could be improved. Due to the layout density of longitudinal reinforcement, it is difficult to significantly improve the reinforcement ratio in the actual engineering project. Hence, the application of high-strength reinforcement in the precast bridge column connected with GCMD is worth further study. However, the influence of the concrete strength had little influence on the ultimate strength, ultimate deformation capacity, residual deformation and energy dissipation capacity. Therefore, the concrete strength of precast bridge columns connected with GCMD can be taken as the design value under normal loads.

The above comprehensive research results are believed to potentially benefit the seismic design of precast bridge columns connected with GCMD that are subjected to bi-directional load. A future study could focus on the full-scale test of the precast bridge column connected with GCMD.

Conflicts of interest

The authors declare that there is no conflict of interest regarding the publication of this paper.

Acknowledgment

The authors gratefully acknowledge the financial support provided by the Natural Science Foundation of China (NSFC) under Grant No. 51408360, the Natural Science Foundation of Fujian (NSFF) under Grant No. 2020J01477 and the Technology Project of Fuzhou Science and Technology Bureau (TPFB) under Grant No. 2020-GX-18. The authors′ views and opinions expressed in this paper do not necessarily reflect the views of NSFC, NSFF, and TPFB.

References

AASHTO (2017), *LRFD Bridge Design Specifications*, American Association of State Highway and Transportation Officials, 8th edition, Washington D.C., USA.

ASTM (2011), *Standard Test Method for Splitting Tensile Strength of Cylindrical Concrete Specimens*, C496/C496M, ASTM, Washington D.C., 1–5.

Bae S (2005), "Seismic Performance of Full-Scale Reinforced Concrete Columns," *Doctoral Dissertation*.

Brenes FJ, Wood SL and Kriger ME (2006), *Anchorage Requirements for Grouted Vertical-Duct Connectors in Precast Bent Cap Systems*, Report No. FHWA/TX-06/0-4176-1, University of Texas, Austin, Texas, USA.

Chan M, Poon WK, Leung YW, Chan DSH, Premaud V and Rialland Y (2016), "Challenges in Hong Kong–Zhuhai–Macao Bridge (HZMB) Hong Kong Link Road Project," *International Association for Bridge and Structural Engineering*, Taylor & Francis, **106**(4): 797–804. DOI: 10.2749/222137816819259202.

CJJ166-2011 (2011), *Code for Seismic Design of Urban Bridges*, Ministry of Housing and Urban-Rural Development of the People′s Republic of China, China Architecture and Building Press, Beijing, China. (in Chinese)

Darwin D and Zavaregh SS (1996), "Bond Strength of Grouted Reinforcing Bars," *ACI Structural Journal*, American Concrete Institute, **93**(4): 486–495.

DG/TJ 08-2160-2015 (2015), *Technical Specification for Prefabricated Bridge Piers*, Shanghai Urban and Rural Construction and Management Committee, Tongji Press, Shanghai, China. (in Chinese)

Elsayed M, Nehdi ML, Provost-Smith DJ and Eissa OS (2018), "Exploratory Investigation of Grouted Bar-In-Duct Connections Under Direct Tensile Load," *Construction and Building Materials*, **183**: 311–324.

GB/T 228.1-2010 (2010), *Metallic Materials–Tensile Testing– Part 1: Method of Test at Ambient Temperature*, General Administration of Quality Supervision, Inspection and Quarantine of the People′s Republic of China, China National Standardization Administration, Beijing, China. (in Chinese)

GB/T 50152-2012 (2012), *Standard for Test Method of Concrete Structure*, Ministry of Housing and Urban-Rural Development of the People′s Republic of China, China Architecture & Building Press, Beijing, China. (in Chinese)

JGJ/T101-2015 (2015), *Specification of Testing Methods for Earthquake Resistant Building*, Ministry of Housing and Urban-Rural Development of the People′s Republic of China, China Architecture and Building Press, Beijing, China. (in Chinese)

JGJ/T3362-2018 (2018), *Specification for Design of Highway reinforced Concrete and Prestressed Concrete Bridges and Colvers*, Ministry of Transport of the People′s Republic of China, China Communication Press, Beijing, China. (in Chinese)

JTG/T B02-01-2008 (2008), *Guidelines for Seismic Design of Highway Bridge, Ministry of Transport of the People's Republic of China*, China Communication Press, Beijing, China. (in Chinese)

Khaleghi B, Schultz E, Seguirant S, Marsh L, Haraldsson O, Eberhard MO and Stanton JF (2012), "Accelerated Bridge Construction in Washington State: from Research to Practice," *PCI Journal*, Precast/Prestressed Concrete Institute, **57**(4): 34–49. DOI: 10.15554/pcij.09012012.34.49.

Lehman D, Moehle J, Mahin S, Calderone A and Henry L (2004), "Experimental Evaluation of the Seismic Performance of Reinforced Concrete Bridge Columns," *Journal of Structural Engineering*, **130**(6): 869–879.

Li C, Hao H and Bi KM (2018), "Seismic Performance of Precast Concrete-Filled Circular Tube Segmental Column Under Biaxial Lateral Cyclic Loadings," *Bulletin of Earthquake Engineering*, Springer Netherlands, **17**(1): 1–26. DOI: 10.1007/s10518-018-0443-4.

Marriott D, Pampanin S and Palermo A (2011), "Biaxial Testing of Unbonded Post-Tensioned Rocking Bridge Piers with External Replaceable Dissipaters," *Earthquake Engineering & Structure Dynamics*, John Wiley & Sons Ltd, **40**(15): 1723–1741. DOI: 10.1002/eqe.1112.

Menegotto M and Pinto PE (1973), "Method of Analysis for Cyclically Loaded Reinforced Concrete Plane Frames Including Changes in Geometry and Non-Elastic Behavior of Elements Under Combined Normal Force and Bending," *Proc. of Symposium on the Resistance and Ultimate Deformability of Structures Acted on by Well-Defined Repeated Loads*, Taylor & Francis, Lisbon, Portugal.

Motaref S, Saiidi MS and Sanders D (2011), *Seismic Response of Precast Bridge Columns with Energy Dissipating Joints*, Report No. CCEER-11-01, University of Nevada, Reno, Nevada, USA.

Ozcebe G and Saatcioglu M (1987), "Confinement of Concrete Columns for Seismic Loading," *ACI Structural Journal*, **84**(4): 308–315.

Palermo A and Mashal M (2012), "Accelerated Bridge Construction (ABC) and Seismic Damage Resistant Technology: A New Zealand challenge," *Bulletin of the New Zealand Society for Earthquake Engineering*, New Zealand, **45**(3): 123–134.

Pang JBK, Eberhard MO and Stanton JF (2010), "Large-Bar Connection for Precast Bridge Bents in Seismic Regions," *Journal of Bridge Engineering*, ASCE, **15**(3): 231–239. DOI: 10.1061/(ASCE)BE.1943-5592.0000081.

Park R (1989), "Evaluation of Ductility of Structures and Structural Assemblages from Laboratory Testing," *Bulletin of the New Zealand National Society for Earthquake Engineering*, New Zealand, **22**(3): 155–166.

Peng J, Wong LNY and Teh CI (2018), "A Re-examination of Slenderness Ratio Effect on Rock Strength: Insights from DEM Grain-Based Modelling," *Engineering geology*, **246**: 245–254.

Qiu FW, Li WF, Pan P and Qian JR (2002), "Experimental Tests on Reinforced Concrete Columns Under Biaxial Quasi-Static Loading," *Engineering Structures*, Elsevier, **24**(4): 419–428. DOI: 10.1016/S0141-0296(01)00108-0.

Qu HY, Li TT, Wang ZQ, Wei HY, Shen JW and Wang H (2018), "Investigation and Verification on Seismic Behavior of precast concrete frame piers used in Real Bridge Structures: Experimental and Numerical Study," *Engineering Structures*, Elsevier, **154**: 1–9. DOI: 10.1016/j.engstruct.2017.10.069.

Raynor DJ, Lehman DE and Stanton JF (2002), "Bond-Slip Response of Reinforcing Bars Grouted in Ducts," *ACI Structural Journal*, American Concrete Institute, **99**(5): 568–576.

Restrepo JI, Tobolski MJ and Matsumoto EE (2011), *Development of a Precast Bent Cap System for Seismic Regions*, NC, USA.

Saatcioglu M and Ozcebe G (1989), "Response of Reinforced Concrete Columns to Simulated Seismic Loading," *ACI Structural Journal*, **86**(1): 3–12.

Scott BD, Park R and Priestley MJN (1982), "Stress-Strain Behavior of Concrete Confined by Overlapping Hoops at Low and High Strain Rates," *ACI journal*, ACI, **79**(1): 13–27. DOI: 10.14359/10875.

Scott MH and Fenves GL (2006), "Plastic Hinge Integration Methods for Force-Based Beam-Column Elements," *Journal of Structural Engineering*, *ASCE*, **132**(2): 244–252. DOI: 10.1061/(ASCE)0733-9445(2006)132:2(244).

Scott MH, Franchin P, Fenves GL and Filippou FC (2004), "Response Sensitivity for Nonlinear Beam-Column Elements," *Journal of Structural Engineering*, *ASCE*, **130**(9): 1281–1288. DOI: 10.1061/(ASCE)0733-9445(2004)130:9(1281).

Shooshtari A, Moghaddam SH and Masoodi AR (2015), "Pushover Analysis of Gabled Frames with Semi-Rigid Connections," *Steel and Composite Structures*, **18**(6): 1557–1568.

Steuck KP, Eberhard MO and Stanton JF (2009), "Anchorage of Large-Diameter Reinforcing Bars in Ducts," *ACI Structural Journal*, **106**(4): 506–513.

Steuck KP, Pang JBK, Eberhard MO and Stanton JF (2007), *Anchorage of Large-Diameter Reinforcing Bars Grouted into Ducts*, Report No. WA-RD 684.1, University of Washington, Washington, USA.

Tazarv T and Saiidi MS (2015), "UHPC-Filled Duct Connections for Accelerated Bridge Construction of RC Columns in High Seismic Zones," *Engineering Structures*, Elsevier, **99**: 413–422. DOI: 10.1016/j.engstruct.2015.05.01.

Tazarv T and Saiidi MS (2016), "Low-Damage Precast Columns for Accelerated Bridge Construction in High Seismic Zones," *Journal of Bridge Engineering*, *ASCE*, **21**(3): 04015056. DOI: 10.1061/(ASCE)BE.1943-5592.0000806.

Tazarv T and Saiidi MS (2017), "Design and Construction of UHPC-Filled Duct Connections for Precast Bridge Columns in High Seismic Zones," *Structure and Infrastructure Engineering*, *ASCE*, **13**(6): 743–753. DOI: 10 .1080/15732479.2016.1188969.

Wacker JM, Hieber DG, Stanton JF and Eberhard MO (2005), *Design of Precast Concrete Piers for Rapid Bridge Construction in Seismic Regions* (No. WA-RD 629.1), University of Washington, Washington, USA.

Wang JC, Ou YC, Chang KC and Lee GC (2010), "Large-Scale Seismic Tests of Tall Concrete Bridge Columns with Precast Segmental Construction," *Earthquake Engineering and Structural Dynamics*, **37**(12): 1449–1465.

Wang ZQ, Qu HY, Li TT, Wei HY, Wang H, Duan HL and Jiang HX (2018), "Quasi-Static Cyclic Tests of Precast Bridge Columns with Different Connection Details for High Seismic Zones," *Engineering Structures*, Elsevier, **158**: 13–27. DOI: 10.1016/j.engstruct.2017.12.035.

Xu S, Wu C, Liu Z, Han K, Su Y, Zhao J and Li J (2017), "Experimental Investigation of Seismic Behavior of Ultra-High Performance Steel Fiber Reinforced Concrete Columns," *Engineering Structures*, **152**: 129–148.

Zhuo W, Liu Z, Zhang J and Zhang W (2018), "Comparison Study on Hysteretic Energy Dissipationand Displacement Components Between Cast-in-Place and Precast Piers with High-Strength Bars," *Structural Concrete*, **19**(3): 747–757.